Faculty of Natural Science and Technology
Department of Physics

NTNU
Innovation and Creativity

MASTER'S THESIS FOR

STUD. TECHN. BØRGE AUNE SCHJELDERUPSEN

Thesis started: 01.20.2007
Thesis submitted: 06.18.2007

DISCIPLINE: CONDENSED MATTER PHYSICS

Norsk tittel: *"En reologisk studie av nano-silikater i elektrisk felt"*

English title: *"A Rheological Study of Nano-Layered Silicates in an External Electric Field"*

This work has been carried out at Department of Physics, under the supervision of Professor Jon Otto Fossum

---

Trondheim, 06.18.2007

Jon Otto Fossum

Responsible supervisor

Professor at Department of Physics

Abstract

The rheology of synthetic clays, namely laponite and Na-fluorohectorite, dispersed in silicone oil subject to DC electric field is investigated. Under application of electric fields higher than $\sim$ 500-600 $\frac{\mathrm{V}}{\mathrm{mm}}$, the suspensions change rheological properties from liquid to a solid-like state, due to the formation of chain- and/or column-like structures parallel with the electric field. This effect is called the electrorheological (ER) effect.

In this thesis the yield stresses of clay suspensions at various electric field strengths are measured by two different methods, a standard method and a new method. The standard method gives the static yield stress while the new gives the bifurcation shear stress, which some consider to be the "true" yield stress. The measured yield stresses σ are analyzed in relation to the electric field strengths E and the particle volume fraction Φ, using the power law $\sigma \propto \Phi^{\beta} E^{\alpha}$. For laponite suspensions the exponents found are almost equal for both methods, $\alpha \sim$1.7 and $\beta \sim$1.1.

Only the bifurcation shear stress is measured for NaFH suspensions. Due to problems with large currents, only the most dilute suspension could be measured over a wide electric field range. The electric field dependence obtained for this concentration is α=1.53. The volume fraction dependence of the electric field was not investigated, since exact concentrations were unknown.

The obtained results are consistent with the values predicted by the nonlinear conduction model.

Preface

This report is the result of my work in the course TFY4900 Physics. It is written in my 10th and final semester of my Master of Technology degree (norwegian: "sivilingeniør") at the Department of Physics, Norwegian University of Science and Technology (NTNU). This course corresponds to a work load of 30 points, or one semester.

I would like to thank my supervisor Professor Jon Otto Fossum for help and guidance through the semester.

Trondheim, June 18, 2007 Børge Aune Schjelderupsen

Contents

Chapter 1

Motivation and Outline

This work is a continuance of the work done in my project in the 9th semester, autumn 2006 [1]. The rheology of suspensions of synthetic clays dispersed in silicone oil subject to electric fields is investigated using a rheometer.

For me it has been interesting getting to know more about clays and the surprising complex phenomena that can occur in such systems. Especially, the electrorheological fluids have been fascinating to study. They are perfect examples of a smart material which can change mechanical properties instantaneous with an electric signal, leading to various possible industrial applications. Even though, a great deal of research remains before such applications can be realized.

In addition I have gained an insight into the field of experimental physics. I have realized that the measurements are more complicated than they appear, they take far more time than you expect them to, and that all sorts of problems you fear will happen, usually happens. These experiences will hopefully save me some time in the future.

The master's thesis is organized in the following way: Chapter 2 gives a short general introduction to clays, complex phenomena in clays and the electrorheological effect. In Chapter 3 some general theory about rheology, yield stress fluids, electrorheological fluids and clays are presented. Further in Chapter 4 all relevant experimental details are discussed, including materials used, sample preparation, the experimental setup and the different rheological measurements performed. The results and analysis of the measurement data are presented in Chapter 5. Finally a discussion and conclusion are given in Chapter 6.

Chapter 2

Introduction

Clays and clay minerals have been a part of human everyday life for thousands of years. The traditional use has been as material of many kinds of ceramics such as pottery, porcelain, bricks and tiles [2]. Nowadays clays have a much wider range of application. For example, clays are important rheological modifiers in paints, cosmetics, toothpaste and food production. Clays are also the most important ingredient in modern drilling fluids, making it possible to collect oil and natural gas from reservoirs several kilometers under the sea floor. Clay has also been implicated in the prebiotic synthesis of biomolecules. The optimization the clays' physical and chemical properties opens prospects of using clays for pollution control and environmental protection [2]. It is no wonder why clays are by someone considered to be the material of the 21st century.

There are two main reasons why clays are interesting: (1) their common availability and (2) their extraordinary properties. Clays are naturally occurring nanomaterials, abundant, inexpensive, and environmentally friendly. Clays can be found all over the world. Most clays are a result of the interaction of aqueous solution with rocks. Clays in nature undergo spontaneous modification and transformation as environmental conditions change. These processes are driven by physical, chemical, and biological forces. Natural clays are highly heterogeneous in composition and contain impurities in the form of associated minerals and X-ray amorphous materials. For this reason, most clays used in industrial applications are synthesis of pure minerals in a controlled laboratory environment, referred to as synthetic clays.

Synthetic clays have received much attention from scientists all over the world. There are several reasons for this. First of all, by studying pure synthetic clays we get a better understanding of natural clays. Secondly, to exploit the clay's unique structure and surface properties to new application. The third reason is of a more fundamental character, that is to use synthetic clays as physical model systems in which to study universal physical phenomena within complex systems and materials generally [3]. This is also the objective of this study.

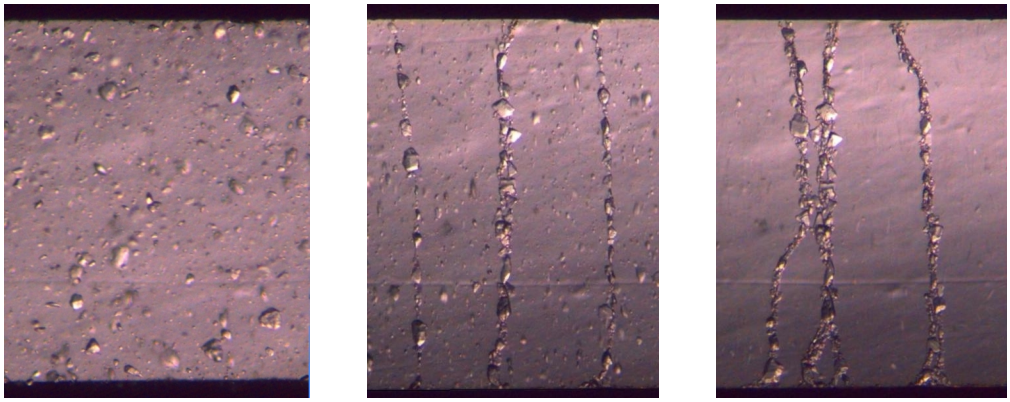

(a) (b) (c)

Figure 2.1: Optical microscope images of chain formation for a laponite/silicone oil suspension in a 1 mm electrode gap when applying different voltages: (a) 0 V, (b) $\sim$ 500 V and (c) $\sim$ 2000 V. Done in collaboration with Svein Åsmund Slungård.

Some interesting phenomena that can be studied by considering synthetic clays are: water transport in nanoporous layered-materials [4] and spontaneous organization of clayparticles in aqueous salt solutions [5]. The latter may give valuable information on how to design real, advanced nano-composite materials.

Another type of organization of clay particles is found when dispersing certain types of clays such as Na-fluorohectorite (NaFH) or laponite in silicone oil or similar oils, and applying an electric field higher than a critical electric field strength, E_c $\sim$500-600 $\frac{\mathrm{V}}{\mathrm{mm}}$, to the system. Clay particles and aggregates will form chain- or column-like structures parallel to the electric field. This form of particle organization can be considered as a "guided organization" as opposed to the spontaneous organization mentioned earlier. The microstructural changes in the clay/silicone oil systems in electric fields can be observed both by visual observation and by measuring the rheological properties, e.g. viscosity, yield stress and storage modulus. This phenomenon will be the subject of this study.

Figure 2.1 shows optical microscope images of a laponite/silicone oil suspension placed between electrodes with 1 mm gap when applying different voltages. When no voltage is applied to the system, Figure 2.1 (a), the aggregates are randomly distributed between the electrodes. In (b) $\sim$ 500 V is applied, and three chains are formed across the electrodes. When applying 2000 V, shown in Figure 2.1 (c), the chains grows thicker and neighboring chain starts to attract each other and eventually form thick column-like structures.

Figure 2.2 shows the result of a rheological measurement on a laponite/silicone oil suspension when applying and turning off an electric field E=1 $\frac{\mathrm{kV}}{\mathrm{mm}}$. The suspension is sheared at a constant shear rate and the measured viscosity is plotted as a function of time. The electric field is applied after 20 seconds and then turned off after another 20

seconds etc. The viscosity of the suspension increases with an order of magnitude when the electric field is applied. This is due to the formation of chains shown in Figure 2.1.

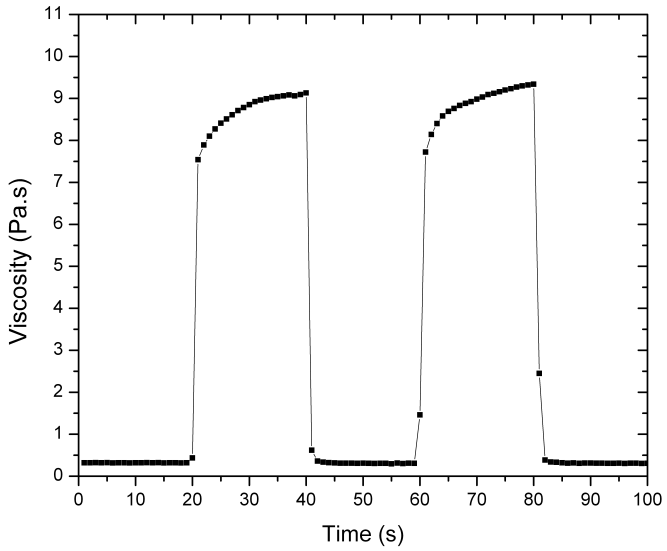

Figure 2.2: The rheological behavior of a laponite/silicone oil suspension sheared at a constant shear rate $\dot{\gamma}$=5 $\frac{1}{\mathrm{s}}$ when applying and turning of an electric field off order 1 $\frac{\mathrm{kV}}{\mathrm{mm}}$. The measured viscosity is plotted as a function of time. The electric field is applied after 20 and 60 seconds, operating for 20 seconds each time before it is turned off.

The microstructural changes that arise when applying an electric field are called the electrorheological effect (ER), and suspensions with these characteristics are referred to as ER fluids. The ER effect was first described by Winslow in 1949 [6], although the phenomenon had been observed already in the late nineteenth century. It was not until the 1980's the subject got a lot of attention and numerous scientific publications concerning the phenomenon started to appear. This was when the industry discovered the potential of using ER fluids in industrial applications.

A typical ER fluid consists of colloid particles suspended in insulating oil. When applying sufficiently high electric fields to the suspension, structural changes can be observed within milliseconds. The response is also reversible, i.e. when switching of the electric field the suspension goes back to its normal state. A generally accepted theory for the ER effect is that the electric field polarizes particles in the dispersion which in turn interacts with each other, thus forming chains parallel to the electric field.

Insulating oils used to prepare ER fluids are silicone oil, vegetable oil, mineral oil, paraffin, kerosene, chlorinated hydrocarbons, transformer oil etc [7]. An ideal dispersing liquid should have low volatility, high chemical stability, high boiling point, low viscosity, high

breakdown strength, relative high density and low dielectric constant. A wide range of solid particles can be used to make ER fluids: clays, organic and polymeric semiconducting materials, carbonaceous materials and superconductive materials [7].

The main motivation for studying ER materials has been the possibility of using them in various industries, especially in the automotive- and robotics industry. The reason for this is that the state of the material can be controlled by an electrical signal, making it a perfect mechanical-electrical interface. Proposed applications are ER clutches, brakes, damping devices, hydraulic valves, smart training equipment etc. Some of these applications have already been patented.

There are several challenges that must be overcome before ER fluids can be used for industrial applications. The main problem with the present ER fluids is that they have too low yield stresses, i.e. they can not handle the stress needed for the industrial applications. There are also problems with the stability of the suspensions due to particle sedimentation, since the ER effect decreases with decreasing particle concentration.

Much progress has been made in preparing ER fluids with high yield stresses. In 2003 Wen et al. reported that barium titanyl oxalate nanoparticles coated with urea dispersed in silicone oil showed a remarkable high yield stress in electric fields [8]. The effect was named giant electrorheological (GER) effect. In high electric fields (E=5 $\frac{\text{kV}}{\text{mm}}$) the system can attain yield stresses higher than 250 kPa [9]. This strength is comparable with what is typical for polyesters. The yield stress attained at moderate electric fields (E=1 $\frac{\text{kV}}{\text{mm}}$) was about 15 kPa. The yield stresses obtained for the clay/silicone oil suspensions studied here are much smaller.

The future of ER fluids and various ER applications depends on a better understanding of the mechanisms involved. With this knowledge it would be possible to choose the most suitable materials, both in terms of yield stress strength, response time and suspension stability. A lot of progress has been made the last decades, but there are still many unanswered questions.

Chapter 3

Theory

3.1 Rheology

The term rheology was introduced by Professor Bingham of Lafayette College, Indiana. It means the science of deformation and flow of matter. This definition was accepted when the American Society of Rheology was founded in 1929 [10].

The definition of rheology suggests that the behavior of all matter can be studied, from Hookean solids to Newtonian viscous liquids. However, these two classical extremes are considered to be outside the scope of rheology [10]. Many materials have both elastic and viscous properties, called viscoelastic behavior, depending on the applied stress and/or the timescale they are observed [11]. Mayonnaise is an example of a material which behaves as a solid for small shear stresses, since it holds its shape under influence of gravity, but starts to flow when subject to larger "squeezing" forces. Window glass is a typical example of a material which behaves differently on different timescales. This is evident when watching windows on old houses and churches where the glass is much thicker at the lower part than at the top. The glass flows, especially at warm days, due to gravity with a large characteristic time. However, most, if not all, people will consider glass to be solid when observing and touching it. This shows that the difference between a liquid and a solid is not as clear as one may think.

Typical materials studied by rheology are polymeric liquids and melts, suspensions of colloidal particles and micellar solutions. Also foodstuffs, pharmaceuticals, cosmetics, paints, plastics, rubber, asphalts and lubricants are materials where the rheological properties plays a major role, and must be known and controlled.

Whether a material is consider being a solid, liquid or something in between depends on the response to an applied stress. In the next sections the stress response for a classical Hookean solid and a Newtonian liquid will be presented .

3.1.1 Hookean Solid

Consider an ideal Hookean solid with the bottom face fixed, as shown in Figure 3.1. A force F is applied to the upper surface with an area A. The resulting shear stress σ, is given by [12]

$$\sigma = \frac{F}{A} = G \tan\gamma \approx G\gamma, \tag{3.1}$$

where γ is the shear angle (strain) and G is the shear modulus. The approximation $\tan\gamma \approx \gamma$ is only valid for small shear angles. G relates to the stiffness of the solid. When removing the force F the original shape of the solid is recovered. This means that the energy required for the deformation is fully recovered when the stress is removed.

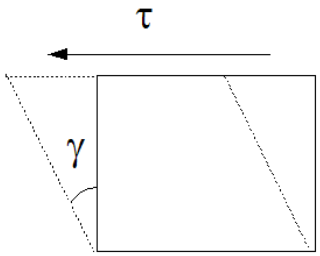

Figure 3.1: A shear stress is applied to a Hookean solid at the upper surface, with the bottom face fixed. This leads to a deformation defined by the shear angle (strain) γ.

3.1.2 Newtonian Liquid

There are many ways of shearing a liquid. The simplest is to use a geometry of sliding plates. In this case an ideal Newtonian liquid is kept between two slightly separated parallel planes with area A , shown in Figure 3.2. A force F gives the upper plane a velocity U in the x-direction, while the other plane is stationary. This leads to a laminar flow with a maximum velocity at the upper surface, which decreases linearly to zero at the lower plate. The shear stress required to produce the motion is [13]

$$\sigma = \eta\frac{U}{d} = \eta\frac{\mathrm{d}v_x}{\mathrm{d}y} = \eta\dot{\gamma}, \tag{3.2}$$

where η is the shear viscosity or simply the viscosity, and $\dot{\gamma}$ is the shear rate.

The energy required for the deformation is dissipated within the fluid in the form of heat and can not be recovered by simply removing the stresses. Therefore, in order to maintain the flow, energy must be added continuously. The viscosity is a measure of a liquid's resistance to flow or internal friction.

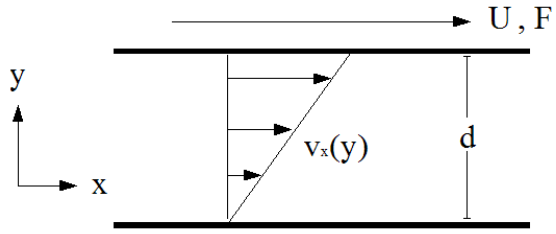

Figure 3.2: Two parallel plates with a ideal liquid between. A force F acts on the upper plane, giving it a velocity U i the x-direction. This creates a laminar flow between the plates.

The viscosity is highly dependent on the temperature T in the liquid. The Arrhenius expression gives an approximation for this relationship for Newtonian liquids [10],

$$\eta(T) = A\mathrm{e}^{-\frac{B}{T}}, \tag{3.3}$$

where A and B are constants of the liquid. The viscosity decreases with increasing temperature. This is why it is very important to control the temperature when doing rheological measurements.

3.1.3 Non-Newtonian Liquids

Generally η is not a coefficient as suggested by Equation (3.2), but a function of the shear rate $\dot{\gamma}$. Liquids with a shear dependent viscosity are called non-Newtonian fluids. Liquids with a viscosity which increases with increasing shear rate are called shear-thickening liquids. Liquids with the opposite behavior are called shear-thinning liquids. Typical non-Newtonian liquids are suspensions, emulsions and polymer solutions.

3.1.4 Basic Principles of Rotational Rheometers/Viscometers

A viscometer is an instrument for measurement of shear viscosity only, while a rheometer is a instrument for measuring rheological properties in general. One can say that the rheometer is a more sophisticated and advanced version of the viscometer. A rheometer is able to produce both steady shear and oscillating motion among other things. I will give a brief introduction to how rotational concentric-cylinder viscometers work, since the principles are the same as for the rheometer.

Rotational concentric-cylinder viscometers relay on rotation motion to achieve a simple shearing flow [10]. This can be done in two different ways: rotating the inner cylinder while the outer is stationary, or rotating the outer cylinder while the inner is stationary.

The first method is called a Searle type measuring system and the second a Couette measuring system.

Searle Type Measuring System

For the Searle type measuring system there are two different methods the viscosity can be measured [13]:

1. The inner cylinder, rotor, is driven by a motor with defined torque values. The resistance of the sheared sample against the applied torque or shear stress will allow the rotor to rotate at only one speed (shear rate) that inversely correlates to the viscosity of the sample. The motor speed n and the strain position ϕ can be measure by an optical sensor which divides a 360° revolution into many segments and therefore detect extremely small stain deflection of the rotor. The sensor system is designed in such a way that the torque data can be mathematically transformed to shear stress and the rotor speed to shear rate. Rheometers that use this technique are called controlled shear stress (CSS) rheometers.
2. The rotor is driven by a motor which provides a constant or programmed rotor speed. The resistance of sheared liquid results in a viscosity-related torque working on the inner cylinder which counteracts the torque provided by the drive motor. A torque detector, often a spring placed between the motor and the shaft of the inner cylinder, measures the viscosity-related torque. Said in other words, a shear rate is assigned by motor and the corresponding shear stress is measured. Rheometers that use this technique are called controlled shear rate (CSR) rheometers.

Some modern rheometers are able to work in both modes.

Couette Type Measuring System

In the Couette type measuring system there are two motors working. One motor working in CSR-mode rotates the outer cylinder, the cup, while the other is connected to the inner cylinder (measuring bob). The resistance of the liquid against being sheared transmits a viscosity related torque to the inner cylinder, which would induce it also to rotate. The torque is measured by determining just what torque is required to counteract the rotating motion, keeping the measuring bob at standstill.

Concentric Cylinder Systems

If the gap between two concentric cylinders is small enough and the cylinders are in relative rotation, the test liquid enclosed in the gap experiences an almost constant shear rate. If the inner cylinder with radius r_i is rotating at a constant angular velocity ω while the cup with radius r_o is stationary, the shear rate is given by

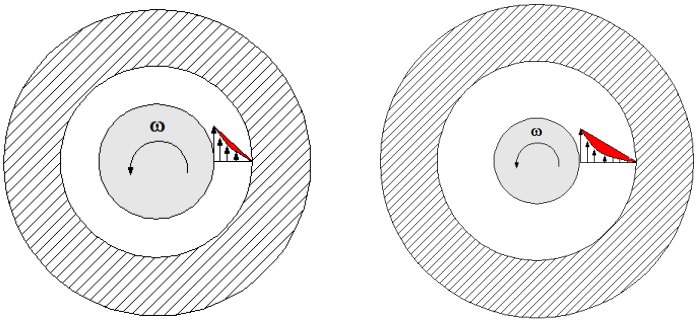

(a) (b)

Figure 3.3: A concentric cylinder system seen from above. The inner cylinder is rotating at a constant angular velocity ω, while the other is stationary. The velocity-field is indicated for (a) a narrow gap system and (b) a wide gap system

$$\dot{\gamma} = \frac{v_{max}}{y} = \frac{\omega r_i}{r_o - r_i}. \tag{3.4}$$

If C is the couple (torque) on the rotating cylinder required to keep it at a constant angular velocity, the shear stress in the liquid is given by

$$\sigma = \frac{F}{A} = \frac{C}{2\pi r_o^2 L}, \tag{3.5}$$

where L is the effective immersed length of the liquid being sheared. This would correspond to the real length of the immersed cylinder, if there were no end effects. If the ratio of the depth of liquid to the gap between the cylinders is larger than 100, end effects become negligible. Alternatively, the end of cylinder can be formed as a cone in such a way that the shear rate in the liquid trapped between the cone and the bottom of the outer cylinder is the same as the liquid between the cylinders.

The shear viscosity is then given by

$$\eta = \frac{\sigma}{\dot{\gamma}} = \frac{C(r_o - r_i)}{2\pi r_o^3 \omega L}. \tag{3.6}$$

However, the situation for most real concentric cylinder systems is that the gap between the outer and the inner cylinder is too big to give a perfect laminar flow in the gap. Instead there is a non-linear velocity-field in the gap, which becomes more dominating with increasing gap size. This is illustrated in Figure 3.3. The ratio of the radii $\delta = \frac{r_o}{r_i}$ is often used as a measurement of how large the non-linear effects are. The closer the ratio is 1, the better it is rheologically. For dispersions with large particles, a very narrow gap is not favorable. Most concentric cylinder systems are made as a compromise between these two facts, thus some manipulation of the data is needed to produce the right viscosity.

3.2 Yield Stress Fluids

Fluids that do not flow unless they are subject to a certain load, so-called yield stress fluids, are both important in our everyday life and in industrial applications. Some typical examples are mayonnaise, ketchup, toothpaste, shaving foams, gels, paints, concrete and drilling fluids. Common for all of these materials are that they behave as solids for small applied stresses and as liquids at high stresses.

The flow behavior of yield stress fluids under shearing deformation can be described by [14]

$$\begin{aligned} \sigma &= \sigma_y + f(\dot{\gamma}) \ \text{ for } \ \sigma > \sigma_y \\ \dot{\gamma} &= 0 \ \text{ for } \ \sigma < \sigma_y \end{aligned} \tag{3.7}$$

where σ is the applied shear stress, σ_y is the yield stress and $f(\dot{\gamma})$ some function of the shear rate, satisfying $f(0) = 0$ and $\frac{\mathrm{d}f}{\mathrm{d}\dot{\gamma}} > 0$.

A special function form of $f(\dot{\gamma})$ is the so-called Herschel-Bulkley (H-B) model, $\sigma = \sigma_y + a\dot{\gamma}^n$, where a and n are positive constants. In the special case $\sigma_y = 0$ and $n = 1$ the H-B model describes a Newtonian liquid with viscosity a.

From the H-B model we see that the viscosity diverges as the shear stress reaches the yield stress point from above, viz.

$$\eta = \frac{\sigma_y + f(\dot{\gamma})}{\dot{\gamma}} \rightarrow \frac{\sigma_y}{\dot{\gamma}} \text{ when } \dot{\gamma} \rightarrow 0. \tag{3.8}$$

The concept of the yield stress is easy to understand, it is the stress at which the fluid just starts/stops flowing, i.e. where the viscosity changes from a finite value to an infinite. However, to actually measure and determine the yield stress has proven to be very difficult. First of all, in order to distinguish between finite and infinite viscosities, experiments of infinite duration are required. This is of course practical impossible. From the experimentalist point of view the definition of the yield stress must be modified to the highest stress at which no flow is detectable within the duration of the experiment. So the measured yield stress is somewhat dependent of the patience of the experimentalist and the experimental protocol [15].

Another and perhaps more "serious" problem with measuring the yield stress is that different tests often give different results depending on which geometry and experimental procedure used. Variations in the yield stress of more than one order of magnitude has been reported depending on the way it was measured [16]. The solution to this has been to introduce several yield stresses such as the static and the dynamic yield stress. This is of course in conflict with the definition of the "true" yield stress.

The yield stress mechanism is mostly due to the microstructure of the fluid that resists large rearrangements. The system is jammed and starts or stops flowing abruptly. When

the fluid is subject to a shearing force the microstructure is partly destroyed. This is evident in rheological tests, where the viscosity of the fluid decreases over time, so-called thixotropic behavior. At rest the microstructure of most of the yield stress fluids, reforms or evolves spontaneously, the system is said to age. This will lead to an increase in the apparent yield stress with time. Thus, the mechanical behavior of these systems under shearing is result of the competition between aging and the destruction of the microstructure by the shear flow.

Bonn et al. showed that the typical yield stress fluids start flowing abruptly and subsequently accelerate, leading to avalanches similar to those in granular materials [17]. This was done by performing inclined plane tests of aqueous clay suspensions. When the thickness h of the deposited material is much smaller than its extent over the plane, the shear stress distribution at rest is [18]

$$\sigma = \rho g(h - y)\sin(\theta), \tag{3.9}$$

where y is the height above the plane, ρ is the density of the material, g is the gravitational acceleration and θ is the slope of the plane.

For an ideal yield stress fluid the flow stops when the maximum shear stress along the plane becomes equal to the yield stress σ_y, i.e. when $h = \frac{\sigma_y}{\rho g \sin(\theta)}$.

The inclined plane tests revealed that for a given thickness of the initial deposit there exist a critical slope (corresponding to a critical stress) below which the aging dominates over the destruction of the microstructure, leading to that the fluid stops moving much faster than an ideal yield stress fluid. For slightly higher slopes the destruction of microstructure fluidizes the sample, giving a stronger flow, which in turn decreases the viscosity and further accelerating the flow: an avalanche results. The same behavior was also found when they performed the same experiments using sand.

Rheological tests showed that the avalanche behavior was associated with a bifurcation in the rheological behavior. For small stresses the viscosity increases in time, eventually stops flowing. For slightly larger stresses the viscosity decreases continuously in time, indicating that the flow accelerates. At a critical stress the viscosity jumps in a discontinuous way to infinity, as opposed to what was anticipated for yield stress fluids. In addition they found that the critical stress is not an intrinsic property of the sample, since the microstructure of the yield stress fluid depends on the shear history of the sample.

The following model was proposed by Bonn et.al to describes the competition between aging and shearing deformation [17]. The degree of jamming in the system is described by single parameter λ. For an aging system at rest, λ increases at a constant rate $\frac{1}{\tau}$, where τ is the characteristic time of evolution of the structure. The rate of decreases under shearing is assumed to be proportional to both the shear rate $\dot{\gamma}$ and λ. Thus the evolution equation for λ is

$$\frac{\mathrm{d}\lambda}{\mathrm{d}t} = \frac{1}{\tau} - \alpha\lambda\dot{\gamma}. \tag{3.10}$$

The viscosity function is assumed to be

$$\eta = \eta_0(1 + \lambda^n), \tag{3.11}$$

which goes toward η_0 when the structure is entirely destroyed.

In steady-state, $\frac{\mathrm{d}\lambda}{\mathrm{d}t} = 0$ in Equation (3.10) it follows that $\lambda = 1/\alpha\tau\dot{\gamma}$, so the shear stress is given by

$$\sigma = \eta\dot{\gamma} = \eta_0\dot{\gamma}\left[1 + (\alpha\tau\dot{\gamma})^{-n}\right]. \tag{3.12}$$

When $n < 1$, $\frac{\mathrm{d}\tau}{\mathrm{d}\lambda}$ is always positive, but the fluid has no yield stress since $\tau \to 0$ when $\dot{\gamma} \to 0$. This corresponds to simple shear-thinning behavior. For $n \geq 1$, σ is nonzero when $\dot{\gamma} \to 0$, in other words the fluid has a yield stress. Only in the limiting case $n = 1$ σ goes to a finite value when $\dot{\gamma} \to 0$, i.e. ideal yield stress fluid behavior.

If a constant shear stress is applied (substituting $\dot{\gamma}$ from Equation (3.12)) to Equation (3.10) we get

$$\frac{\mathrm{d}\lambda}{\mathrm{d}t} = \frac{1}{\tau} - \frac{\alpha\lambda\sigma}{\eta_0(1 + \lambda^n)}. \tag{3.13}$$

The variations of λ, and thus the viscosity variations are dictated by the relative values of the two terms on the right-hand side of Equation (3.13). The initial state of the structure is assumed to be $\lambda(t = 0) = \lambda_0$. The time-dependent solution to this equation, shown in Figure 3.4, reproduces the bifurcation observed in experiments.

3.3 Electrorheology

The mechanisms behind electrorheology are mainly considered to be a result of particle polarization due to the difference in dielectric constant and/or conductivity between the carrier fluid and the dispersed colloid particles. The resulting electrostatic interaction forces between particles leads to the formation of aggregates aligned in the direction of the electric field. In general the polarization may arise from various mechanisms of charge transport, such as orientation of atomic or molecular dipoles and interfacial polarization, with the latter thought to be the most important in most cases [19].

Also other models have been proposed to describe the microstructural changes ER fluids experience in an electric field. The water bridge model has received some merit because it is able to describe why the ER effect decreases with decreasing water content for some ER-fluids [20–22]. The fact that many ER fluids are anhydrous proves that this

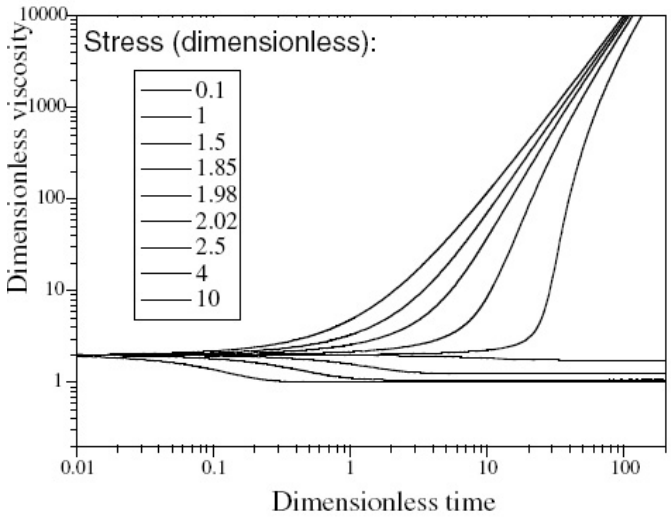

Figure 3.4: Dimensionless viscosity $\frac{\eta}{\eta_0}$ as a function of dimensionless time $\frac{t}{\tau}$ for different applied dimensionless stresses $\frac{\sigma\tau}{\eta_0}$. The following constants are use: n=2, α=1 and λ_0=1 [17].

mechanism can not produce the ER effect alone. Another proposed mechanism is the overlap of the electric double layers [23, 24]. This is however just a special case of the polarization mechanism [25]. An further mechanism proposed is an electrostatic torque preventing particle rotation in the flow field [25, 26]. It is possible that some of these mechanisms play a role in the ER effect together with the polarization mechanism, but these will not be discussed further here.

The ultimate goal is to develop a theory for the ER effect which accurately describes the eleastic properties, e.g. yield stress or storage modulus, at a given electric field strength when dispersing a certain type of colloid particles in a given carrier fluid with particle volume fraction Φ. This is very ambitious since most ER fluids involve many particles with complicated structure and electric properties. The starting point for most computer simulations is a small number of the simplest particles, i.e. spherical particles with constant dielectric constant and conductivity, in a simple carrier fluid. The equation of motion is then simulated by considering the relevant forces acting on each particle.

The most important forces acting between particles are electrostatic forces due to polarization of particles and a rigid body repulsion [19, 27]. The latter is often approximated by a soft-core potential [19]. The dispersed particles also experience a hydrodynamic interaction, a drag force, as they move through the carrier fluid with viscosity η. This force depends on the relative positions of other particles and their velocities and orientation with the respect to externally applied flow field. Simulations often use different external flow fields $\dot{\gamma}(t)$ such as no flow, very small shear rates, steady shear rate and small amplitude oscillatory shear. The electrode wall interaction force is also included

in most simulations. Usually Brownian motion effects are ignored in simulations, except when simulating very small particles. Gravitational forces are also usually ignored.

Here I will only discuss some aspects of particle polarization and approximation used to evaluate the electrostatic interaction between particles. The interparticle forces will also be related to the yield stress, giving the electric field- and particle volume fraction dependence.

3.3.1 Basic Mechanisms

Consider an isolated sphere of radius a with dielectric constant ϵ_p and conductivity K_p suspended in a carrier fluid with dielectric constant ϵ_f and conductivity K_f. This system is placed between a pair of parallel electrodes separated by a distance of h_0. A constant or an alternating voltage is applied to the electrodes, inducing a DC or AC electric field. The electric field will then polarize the sphere.

In the idealized electrostatic polarization theory it is assumed that the conductivity of the particle and carrier fluid are zero, i.e. $K_p = K_f = 0$, and that a DC electric field $\vec{E} = E_0\hat{e}_z$ is applied. To determine the electrostatic forces in the system, the electrostatic potential Ψ must be found. This can be done by solving the Laplace's equation, $\nabla^2\Psi = 0$, for the boundary conditions at the sphere/fluid interface, i.e. $\Psi^p{=}\Psi^f$ and $\epsilon_p\nabla\Psi^p{=}\epsilon_f\nabla\Psi^f$ [28]. By solving these equations and remembering that $\vec{E}(r) = -\nabla\Psi$ it can be shown that the electric field outside the particle is the same as for an electric dipole located at the particle center [27]. The magnitude of the dipole moment is given as

$$P_{diel} \propto a^3\epsilon_0\epsilon_f\beta_{diel}E_0, \tag{3.14}$$

where

$$\beta_{diel} = \frac{\epsilon_p - \epsilon_f}{\epsilon_p + 2\epsilon_f} \tag{3.15}$$

and ϵ_0 is the permittivity of free space.

In the case of non-zero conductivities, but $K_p >> K_f$, β_{diel} in Equation (3.14) is replaced by

$$\beta_{cond} = \frac{K_p - K_f}{K_p + 2K_f}. \tag{3.16}$$

This model is called the conduction theory [29–31].

In both these models the polarized particles can be approximated by a dipole. However, it turns out that the relevant physical properties (dielectric constants or conductivities) depends on the nature of the applied electric field. Under DC and low frequency AC conditions, the degree of polarization depends on the conductive properties [31, 32]. In high frequency AC electric field the dielectric constants are the governing properties. At

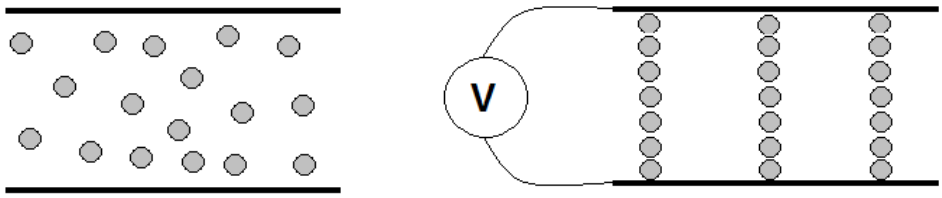

(a) (b)

Figure 3.5: Schematic illustration of microstructure change of an ER fluid before (a) and after (b) an external electric field is applied

intermediate frequencies both permittivity and conductivity play a role. The Maxwell-Wagner model is the simplest description of particle polarization accounting for both [19,27,33].

In the case of many spherical particles present in the carrier fluid it is difficult to exactly calculate the electrostatic interaction force experienced by particle i due to particle j. The simplest approximation to this problem is the point-dipole approximation assuming pairwise interactions [19,27]. It is also assumed that the particles are well separated so that particles do not alter each other's charge distribution. The force $\vec{F}_{elec}^{ij}$ acting on particle i with polarization P_i due to another particle j is given by

$$\vec{F}_{elec}^{ij}(t) = \vec{P}_i \nabla \vec{E}_j, \tag{3.17}$$

where $\vec{E}_j$ is the disturbance field created by particle j. The result of the calculation given in polar coordinates is

$$\vec{F}_{elec}^{ij}(t) = F_s(t)\left(\frac{a}{r_{ij}}\right)^4 [(3\cos^2\theta_{ij} - 1)\hat{e}_r + 2\sin\theta_{ij}\hat{e}_\theta], \tag{3.18}$$

where $F_s(t)$ is the magnitude of force which depends on the nature of the electric field. In the case of a DC electric field, the force magnitude of Equation (3.17) is given by [19]

$$F_s \propto \epsilon_f \epsilon_0 a^2 E_0^2 \beta_{cond}^2. \tag{3.19}$$

The anisotropic character of Equation (3.18) suggest that particles will form chains in an electric field. Figure 3.5 shows a schematic drawing of the chain formation. Particles parallel to the electric field will attract each other and particles perpendicular to the electric field will repel each other. When the line-of-centers are at some angle with respect to the applied field, the pairs will experience a torque attempting to align them with the field.

Another thing is that the force between particles is proportional to β_{cond}^2. By maximizing β_{cond}, i.e maximizing dielectric or conductive mismatch between particles and fluid, one should get maximum particle-particle interaction and thus the strongest ER effect. Experiments have shown that this is not the case. Equation (3.18) captures the essential characteristics of the ER effect, however it greatly underestimates the magnitude of forces when two particles are in close proximity. Higher order electrostatic moments must be included in the calculations. The interaction forces are not pairwise additive when particles are close. For example, the presence of a nearby third sphere greatly alters the interaction forces between a pair of spheres.

The conduction model has been modified to account for increasing conductivity due to nonlinear effects in the narrow interparticle gaps in high DC electric field strengths [34] [35]. In this theory the particle-particle interaction scales linearly with the applied electric field at large electric field strengths [36].

3.3.2 Modeling the Yield Stress

Based upon the electrostatic interaction forces between particles calculated by using the models described in the previous section it is natural to try modeling the rheological properties of ER fluids. A particular interesting property used to determine the strength of the ER effect is the yield stress. The yield stress is usually modeled as a function of the particle volume fraction Φ and the electric field strength E by the power law

$$\sigma_y \propto \Phi^{\beta} E^{\alpha}, \tag{3.20}$$

where the indices α and β take values between 1 and 2 depending on the model used. In the simple polarization theory and Maxwell-Wagner theory the exponents take the values α=2 and β=1 [19,37]. In the DC conduction model which takes into account nonlinear effects, α takes the value 2 at low electric field strengths and 1.5 at higher electric field strengths [36]. Generally α-values less than 2 are reported in the literature both in simulations and experiments. The dependence of volume fraction, β, of the yield stress has not been investigated thoroughly in the literature. Although some have reported β-values varying significantly from the linear relationship predicted by the polarization theory [38,39].

3.3.3 Effect of Particle Size and Shape

The effect of particle size on the ER effect is of great practical interest. If the particles are too small they will experience large Brownian motion effects competing with the chain formation process. On the other hand, if the particles are too large they will sediment rapidly due to gravity [19]. Particle sizes ranging from 0.1 μm to 100 μm have been used to prepare ER fluids. The influence of particle size on the ER effect is quite diverse. For spherical particles it is found that the yield stress increases with

increasing particle size [40]. When mixing small and large spherical particles it was found that shear yield stress decreased compared to suspensions with monodisperse particles, reaching a minimum when the volume fraction of the small particles equals that of the large particles [41].

compared to suspensions with monodisperse particles

The ER effect of non-spherical particles has been investigated primarily in experiments. Some have reported that suspensions of particles with a shape anisotropy reveals a higher yield stress than that of spherical particles at the same volume fraction [42]. They also reported that a mix of spherical and elongated particles will produce higher yield stresses. Experiments on cylindrical fibers with different aspect ratios showed that the ER effect increased significantly with aspect ratio [43].

Mica, a layered flake-formed irregular structure with thickness 1 μm and four different particle sizes (45-195 μm), has also been investigated [44]. They found that the yield stress decreased with an increased particle size at a particle volume fraction of 15 %. At 3 and 5 % however, the yield stress increased with particle size. Further they found that there is an optimum concentration for maximum yield stress. The larger the particle size, the smaller the optimum concentration.

There is no doubt need for further systematic study of the influence of particle shape on the ER effect from a theoretical, experimental and computer simulation viewpoint.

3.4 Clay

3.4.1 Crystallographic Structure of Clays

Clays are a part of the mineral group called phyllosilicates, which again is a subgroup of the silicates. The basic chemical unit of the silicates is the SiO_4 tetrahedron shaped anionic group. The central silicon ion has a positive charge of four while each oxygen atom has a negative charge of two, which gives a net charge of minus four. The oxygen atoms have only used half of their bonding energy in this structure, and are able to form bonds with other SiO_4 groups. This linking of tetrahedron groups can form complicated structures such as single groups, double groups, chains, rings and sheets. These structures are the basis for dividing silicates into subgroups. Phyllosilicates are sheet-shaped structures, i.e. the particles or crystallines are much thinner than they are wide or long.

The phyllosilicates consists of sheets of tetrahedron and octahedral groups. Each tetrahedron consists of a cation, usually Si^{4+}, Al^{3+} and Fe^{3+}, coordinated to four oxygen atoms, and linked to adjacent tetrahedra by shearing three corners to form a infinite two-dimensional structure, a sheet [2]. In this configuration, one oxygen atom is free to bind to other ions. In Figure 3.6 (a) a SiO_4 group is shown, and in (b) two SiO_4 groups are linked together.

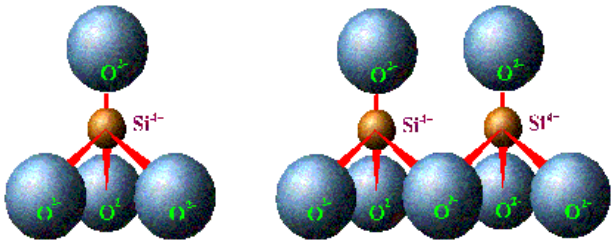

(a) (b)

Figure 3.6: (a) A single tetrahedron SiO_4 and (b) two linked together. Taken from [45]

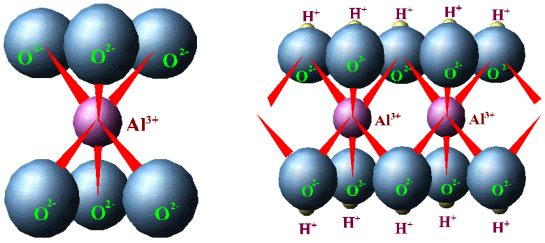

(a) (b)

Figure 3.7: (a) A octahedral AlO_6 and (b) two linked together. Taken from [45]

Aluminum, magnesium or ferrous iron ion, for reasons of coordination, orbit directions and ion diameter, form polyhedra with six oxygen atoms or hydroxyl groups (OH^-) instead of the four oxygen atoms found in polyhedral structures [46]. In the octahedral sheet, connections between each octahedron to neighboring octahedra are made by shearing edges. The edge-shaped octahedra form sheets of hexagonal or pseudo-hexagonal symmetry. Unlike the tetrahedra, in the octahedral linkage the number of cations can vary between two and three. For example, one could have 3 Mg^{2+} ions present or 2 Al^{3+} in the octahedral sites. The basic requirement is that a total positive charge of six is present for the three possible sites. When three ions are present, it is called trioctahedral, and when two cations are present, it is called dioctahedral. The octahedral group AlO_6 and the dioctahedral linkage are shown in Figure 3.7 (a) and (b), respectively. The different sheet structures are shown in Figure 3.8.

The tetrahedral and the octahedral sheet can be linked together through a bridging apical oxygen [46]. The free oxygen atoms in the tetrahedral sheet are sheared with the octahedral anions in the octahedral sheet. The 1:1 layer structure consists of the repetition of one tetrahedral and one octahedral sheet. If one octahedral sheet is "sandwiched" between two tetrahedral the resulting structure is called a 2:1 layer structure. These layer structures are shown in Figure 3.9. In the 1:1 layer structure, the unit cell includes six octahedral and four tetrahedral sites. The unit cell of the 2:1 layer structure consists of six octahedral sites and eight tetrahedral sites. The thickness of the fundamental sheet for the 1:1 structure is 7 Å while the 2:1 structure is about 10 Å thick.

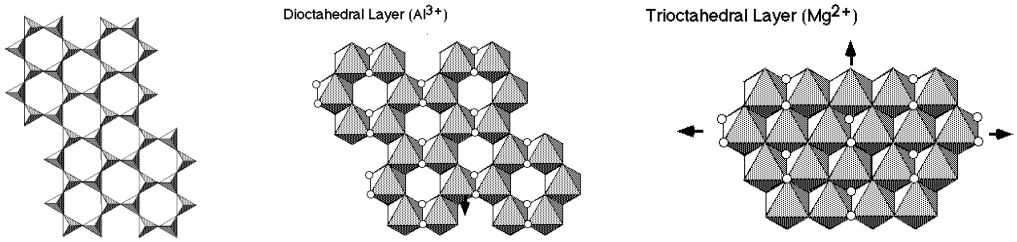

Figure 3.8: Schematic drawing of a (a) tetrahedral sheet , (b) dioctahedral sheet and (c) trioctahedral sheet. Taken from [47]

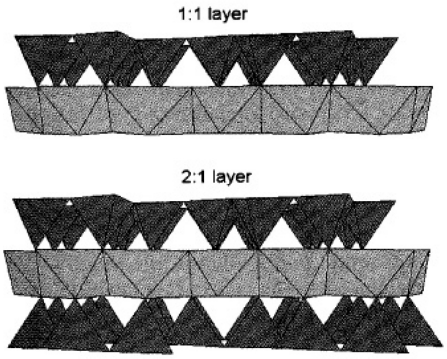

Figure 3.9: The 1:1 layer structure consists of a tetraheral sheet (dark color) linked together with a octahedral sheet (gray color) . The 2:1 layer structure consists of a octahedral sheet "sandwiched" between two tetraheral sheets. Taken from [2]

Most clays are chemically and structurally analogous to other phyllosilicates but contain varying amounts of water and allow more substitution of their cations. There are two different properties of clays which are used to describe and classify clay minerals: their swelling properties and the basic crystallographic repeat unit of the layered structures. Some clay minerals have a special property which allows them incorporate water molecules into their structure. This water changes the dimension of the clay particles as it goes into or out of the clay structure. Clays with these special properties are called expanding or swelling clays. All swelling clays have 2:1 layer structure, but not all 2:1 clays are swelling [48]. The latter and all 1:1 clays are called non-expanding or non-swelling clays. The amount of incorporate water in swelling clays depends on the ambient water vapor pressure and temperature [46].

3.4.2 Smectites

Smectites is the name used for a specific group of the 2:1 swelling clays. Clays that belongs to this group have moderate negatively charged layers, from 0.2 to 0.6 per half-unit-cell [2], due to the substitution of ions in the tetrahedral or octahedral sites, or empty sites (vacancies). The low charge in smectites allows hydrated ions and polar ions to be inserted between the layers (adsorbed). The octahedral layer can either be dominantly occupied by trivalent cations[1] (dioctahedral smectites) or divalent cations[2] (trioctahedral smectites). Species of smectites may be differentiated by: (1) dioctahedral or trioctahedral nature of the octahedral layer, (2) predominant octahedral cation and (3) density and location of the layer charge. Montmorillonite, Beidellite and Nontronite are examples of the most common dioctahedral smectites, while Hectorite and Saponite are the most common trioctahedral smectites.

Commonly Si^{4+}, Al^{3+} and Fe^{3+} are found in tetrahedral sites [2]. When Si^{4+} is replaced by R^{3+} in the tetrahedral sites, this creates an excess of negative charge in the three basal oxygens and the apical oxygen. This affects the total charge of the 2:1 layer as well as the local negative charge at the layer surface. Cations such as Al^{3+}, Fe^{3+}, Fe^{2+}, Mg^{2+}, Ni^{2+}, Zn^{2+} and Li^{+} generally occupy octahedral sites in smectites. In dioctahedral smectites, substitution of divalent cations for trivalent cations creates an excess of negative layer charge, whereas substitution of trivalent for divalent cation in trioctahedral smectites generates an excess of positive charge.

In dry state smectites stack like a deck of cards by shearing charge-compensating cations [48]. Cations usually found in the interlayers are Na^{+}, K^{+}, Ca^{2+} and Mg^{2+}.

[1] ions on the form R^{3+}
[2] ions on the form R^{2+}

Chapter 4

Experimental

4.1 Materials

4.1.1 Laponite

Laponite RD purchased from Laporte Ltd. was used in these experiments. Laponite is a synthetic hectorite clay, with a specific particle density of $\rho_s = 2.65$ [49]. Figure 4.1 shows the idealized structure for a laponite unit cell. This shows six octahedral magnesium ions sandwiched between two layers of four tetrahedral silicon atoms. These groups are balanced by twenty oxygen atoms and four hydroxyl groups. In practice some of the magnesium ions are replaced by lithium ions and some spaces are empty, giving a charge deficiency of 0.7 per unit cell. The approximate empirical formula is $Na^+_{0.7}[Li_{0.3}Mg_{5.5}Si_8O_{20}(OH)_4]^{0.7-}$ [50]. The unit cell is repeated many times in two dimensions, giving laponite a well defined shape and size, a disc-shaped particle with a thickness of approximately 1 nm and diameter of 25-30 nm [50–52]. A single laponite particle is shown in Figure 4.2. The monodisperse shape of the laponite particle makes it a particularly interesting system to study phase behavior of disk-like particles. Natural and other synthetic clays are in general much bigger ($\sim \mu$m) and polydisperse.

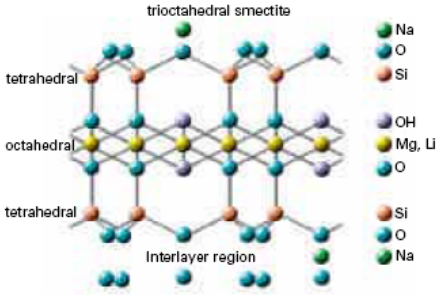

Figure 4.1: Idealized structure formula of a laponite unit cell. Taken from [50].

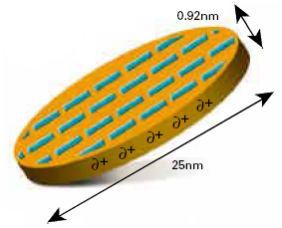

Figure 4.2: A single laponite particle. Taken from [50].

4.1.2 Na-fluorohectorite

Synthetic smectite Na-fluorohectorite (NaFH) purchased from Corning Inc. in powder form was also used in experiments. The clay has the chemical formula $Na_{-0.6}\left[Mg_{-2.4}Li_{-0.6}\right]Si_4O_{10}F_2$ per half unit cell, where Na is an interlayer exchangeable cation [53]. NaFH has a high surface charge, -1.2 e per unit cell [5]. The particle size of NaFH is a quite large and variable with diameters up to 2 μm.

4.1.3 Silicone Oil

The silicone oil used was Dow Corning 200 fluid 100 cS. The oil has a viscosity of 100 cS (=100 mPa·s) and a specific particle density of 0.973 at 25 °C. It is thermally stable, non-flammable and an excellent insulating liquid $\sigma_f(0)$=$5.0{\cdot}10^{-12}\frac{\mathrm{S}}{\mathrm{m}}$ [54]. These properties make it a suitable carrier fluid for ER-fluids.

The chemical structure of silicone oils is similar to hydrocarbons, but instead of the pure carbon-skeleton in hydrocarbons, silicone oils have a silicon-oxygen-skeleton. Two methyl groups (CH_3) are attached to each silicon atom. The chemical name for these polymers is polydimethylsiloxanes. The size of the polymer is usually between 15 and 1,000 monomer units [55]. Figure 4.3 shows the chemical structure of a general polydimethylsiloxane, where n is the number of monomer units.

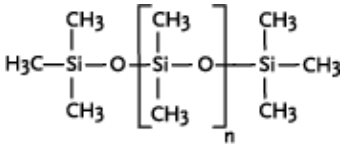

Figure 4.3: The chemical structure of polydimethylsiloxanes. n is the number of monomer units.

4.2 Sample Preparation

4.2.1 Laponite Suspensions

Samples are prepared by heating both the laponite and the silicone oil at 130 °C for 72 hours. This is done to make sure that there is no trace of water left in the samples. Immediately after the heating, the appropriate amount of laponite is mixed with 50 ml silicone oil, sealed and then cooled down to room temperature. The samples were then shaken and put in an ultrasonic bath for 30 minutes. Before a sample was used in rheological measurement, it was shaken vigorously for about 5 minutes.

The samples used here were made of a varying amount of laponite, from 3 g to 15 g, dispersed in 50 ml silicone oil. The concentration of suspensions are given by the particle volume fraction Φ, where

$$\Phi = \frac{V_{clay}}{V_{oil}} = \frac{\frac{m_{clay}}{\rho_{clay}}}{V_{oil}}.$$

The density of the laponite powder, ρ_{clay} is about 1 $\frac{\text{g}}{\text{ml}}$

Table 4.1 shows the amount of laponite added to 50 ml silicone oil and the corresponding particle volume fraction.

Table 4.1: Amount laponite added to 50 ml silicone oil and the concentrations.

Mass LP (g)	Φ (%)
3	6
5	10
7.5	15
10	20
12.5	25
15	30

When the laponite was dispersed in oil, no large aggregates could be seen by visual observation. However, optical microscope images such as those presented in Figure 2.1 shows some large aggregates with a size up to $\sim$ 70 μm for the largest dimension. The shapes of the aggregates are highly irregular.

Figure 4.4 shows two samples with the same laponite volume fraction. One of them has been at rest for several hours, while the other has been shaken recently. This shows that the suspensions are not stable, since particles sediment to the bottom of the container.

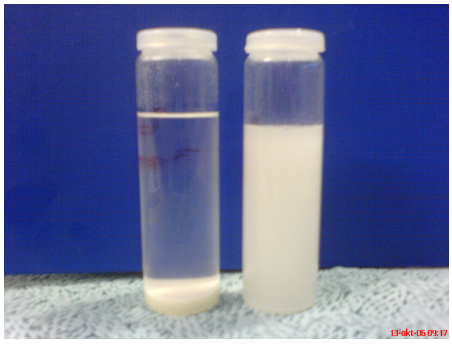

Figure 4.4: Two samples, both made of 3 g laponite and 50 ml silicon oil. The left sample has been at rest for several hours, while the sample to the right has been shaken recently.

4.2.2 NaFH Suspensions

Three NaFH suspensions with different volume fraction were prepared in the same way as described above. An amount of 3, 7 and 10 g NaFH powder were dispersed in 30 ml Dow Corning silicone oil, giving the following volume fractions: Φ= 10, 23 and 33 %. However, in the prepared samples, large aggregates were observed visually. To remove these, the samples were left to rest so that the largest aggregates would sediment to the bottom of the container. The time it took for particles larger than 100 μm to sediment to the bottom was calculated using Stoke's law of particle settling. This gave an approximate time of 10 minutes. After this time the rest of the suspensions were sucked up with a pipette and placed in a new container, leaving only a sediment layer in the original containers. In the new suspensions the clay particles appeared well dispered. The particle volume fractions of the new suspensions were significant lower than in the original. Denoting the volume fraction Φ^*, we remember that this is not the real volume fraction of the suspensions.

4.3 Experimental Setup

4.3.1 Rheometer

The rheometer used in these experiments is a Physica MCR 300 from Anton Paar. It is a rotational rheometer equipped with a permanent magnet synchronous motor with air bearing [56]. Rotational test can be performed both in controlled shear stress (CSS) mode and controlled shear rate (CSR) mode. In addition the rheometer is capable of performing creep tests, normal force tests, stress relaxation tests and different types of oscillatory tests. With a torque range from 0.2 μNm to 150 mNm a wide range of materials from liquids to solids can be investigated.

For electrorheological measurements the Electro Rheological Device (ERD) is used. It consists of coaxial cylinder measuring system (CC27/Q1), standard ISO 3219, coupled

to a high voltage supply (HCN7E-12500), shown schematic in Figure 4.5. The radius of the rotating cylinder is $r_i = 13.33$ mm and the radius of the measuring cup is $r_o = 14.46$ mm, giving a gap of 1.13 mm. The ratio between the outer and the inner cylinder is $\delta = 1.0847$. The gap length L is 39.97 mm, while the cone angle $\alpha_{cone} = 120°$. The sample volume is 19.35 ml. The high voltage supply can deliver voltages from 0 to 12500 V and a maximum current of 0.5 mA.

The ERD is connected to a liquid temperature control system (Viscoterm VT 2) which allows the temperature of the sample to be controlled within 0.1 °C. All measurements performed here are taken at 25 °C. The rheometer, temperature control system and the voltage supply are controlled through the software package US 200.

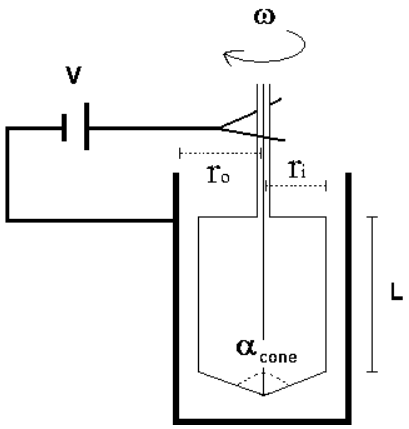

Figure 4.5: Schematic drawing of the Electro Rheological Device

4.4 Rheological Measurements

4.4.1 Effects of Grounding Brushes

The grounding metallic brushes mounted on the protection cover of the ERD shown in Figure 4.5, touches the shaft of the rotating cylinder when doing measurements with an applied voltage. To measure the contribution from the brushes CSR- and CSS tests are performed on the cell containing distilled water. Since water is a low viscous liquid with a viscosity of about 1 mPa·s at 20 °C the tests will be referred to as "empty cell" measurements.

CSR: First an increasing shear rate from $\dot{\gamma}$ =0.1 to 100 $\frac{1}{s}$ is applied to the cell with and without the grounding brushes present while measuring the viscosity. Then constant shear rates (10, 50, 80 and 100 $\frac{1}{s}$) are applied to the cell for 40 seconds with the grounding brushes touching the cylinder shaft. The corresponding viscosities are measured.

(a) (b)

Figure 4.6: The rheometer (a) with the ERD-system (b)

CSR: To check if the brushes contribute to an artificial yield stress an increasing shear stress is applied to the sample with and without the grounding brushes. The shear stress is increased from 0 to 5 Pa in steps of 0.25 Pa while observing the shear rate.

4.4.2 Shear Viscosity

The viscosity as a function shear rate for both laponite- and NaFH suspensions were tested in the the following way: An increasing shear rate from 0 to 1000 $\frac{1}{\text{s}}$ in steps of 20 $\frac{1}{\text{s}}$.

4.4.3 Sedimentation Tests

In order to see how the concentration of the samples changes due to particle sedimentation, CSR tests were performed is the following way: The samples were sheared at a constant shear rate $\dot{\gamma}$= 10 $\frac{1}{\text{s}}$ for 2500 seconds, measuring the viscosity every tenth second.

4.4.4 Static Yield Stress

Static yield stresses for different laponite concentrations and electric field strengths are measured by the same procedure as described by K.P.S Parmar [53].

Samples are first pre-sheared for 100 seconds at a constant shear rate $\dot{\gamma}$=100 $\frac{1}{s}$. Then the electric field is applied for 5 minutes without shearing the sample in order to form chain -or column-like structures across the cylinder gap. Immediately after this an increasing shear stress from 0 to a sufficiently high value, in steps of 1 Pa is applied to the sample. The shear stress where the suspensions start to flow, i.e when a sudden increase in the shear rate emerges, is identified as the static yield stress of the sample for the specific electric field strength. After a measurement the sample is poured back to its container and hand shaken before a new measurement with different electric field strength is performed.

4.4.5 Bifurcation Shear Stress

Attempt has been made to measure the yield stresses of clay ER fluids by the procedure described by Bonn et al. [17], see Section 3.2. This method has given reproducible results for the "true" yield stress for different systems, e.g. gels and clay suspensions. To my knowledge this method has not yet been used to measure yield stresses of ER-fluids.

Each sample is first pre-sheared at a constant shear rate $\dot{\gamma} = 100\ \frac{1}{s}$ for 200 seconds. This is done to makes sure that all samples have the same initial condition (shear history).

Two different procedures were tested in order to determine the bifurcation shear stress of the ER-fluid: (1) Apply an electric field to the sample for 300 seconds without shearing the ER-fluid, and then shear the sample at a constant shear stress for 300 seconds with the electric field still present, while measuring the viscosity. (2) Apply the electric field to the sample and simultaneously shear the sample at a constant shear rate for 300 seconds while measuring the viscosity of the sample.

For procedure (1) the viscosity of the sample either went directly to infinity or toward a low constant viscosity, depending on the magnitude of the applied shear stress. Since the electric field has been applied to the sample before it is sheared, chain- and column-like particle structures are already formed across the gap in the cylinder. These structures have to be broken down in order for the ER-fluid to start flowing, so this procedure is somewhat analogous to the static yield stress procedure presented in Section 4.4.4. However, the shear stress corresponding to the transition between these states was difficult to reproduce, and thus unsuitable as a yield stress point.

Much of the same behavior is found when using procedure (2), however a much more gradual transition between the two states for stresses around a critical shear stress is observed. For shear stresses slightly lower than the critical stress, the sample shows a gradual build-up in the viscosity, suddenly going to infinity. At applied shear stresses slightly above the critical shear stress the viscosity is almost constant over the whole time period. The data produced by this method is reproducible and will therefore be used to measure the yield stress. Following Bonn et al. the critical- or the bifurcation shear stress is taken to be the yield stress of the ER-fluid [17].

After a test has been performed the coaxial measuring cylinder is lifted up and the sample

is stirred with a plastic pipette. This is done to disperse sediment particles again so that the particle concentration is the same for each measurement. A new measurement is then performed with a higher or lower shear stress depending on the outcome of the previous. This procedure is repeated until the bifurcation shear stress for the given laponite concentration and electric field strength is found.

Summary of the procedure used to measure the bifurcation shear stress:

1. Pre-shear the sample at $\dot{\gamma} = 100\ \frac{1}{\mathrm{s}}$ for 200 seconds.
2. Apply an electric field to the sample and start shearing it at a constant shear stress for 300 seconds.
3. Stir up sediment particles
4. Repeat step 1, 2 and 3, but with a higher or lower applied shear stress until the bifurcation shear stress is found

Five different laponite concentrations from $\Phi = 0.1 - 0.3$ are investigated at five different electric field strengths: 0.53, 0.71, 0.89, 1.33 and 1.72 $\frac{\mathrm{kV}}{\mathrm{mm}}$.

The bifurcation yield stress for the three NaFH suspensions are also measured by this technique.

Chapter 5

Results and Analysis

5.1 Empty Cell Measurements

Figure 5.1 shows the measured viscosity as a function of the applied shear rate for the ERD cell containing distilled water, with and without the metallic brushes. Remembering that distilled water only has a viscosity of about 1 mPa·s, it is clear that the grounding brushes greatly contributes to the measured viscosity. The effect is especially evident at low shear rates ($>10\ \frac{1}{s}$) where the measured viscosity is about 100 times larger than it should be. Also at higher shear rates the contribution from the brushes is clear, decreasing towards 10 mPa·s at 100 $\frac{1}{\mathrm{s}}$.

The same can be seen from Figure 5.2, where the viscosity is measured for various constant shear rates with the metallic brushes touching the rotating cylinder. At an applied shear rate of $\dot{\gamma}$=10 $\frac{1}{\mathrm{s}}$ the contribution from the brushes is not uniform, it varies in a zigzag pattern. At higher shear rates however, the contribution from the grounding brushes is almost constant. The extra contribution from the brushes to the measured viscosity is smallest at the highest shear rate.

The conclusion from these measurements is that the brushes give an extra contribution to the measured viscosity. At higher shear rates this contribution can simply be subtracted to get the real viscosity of the sample. The ERD is unsuitable for doing viscosity measurements with applied voltages at low shear rates ($<20\ \frac{1}{\mathrm{s}}$) since the contribution from the brushes is non-uniform and can not simply be subtracted.

Figure 5.3 shows the flow curve of distilled water with and without the grounding brushes present. Here an increasing shear stress from 0 to 5 Pa has been applied. Without the brushes the increased shear stress almost instantly leads to a increased shear rate, but with the grounding brushes present the response is delayed with about 1 Pa. The grounding brushes lead to an artificial yield stress of about 1 Pa which must be subtracted when doing similar measurements.

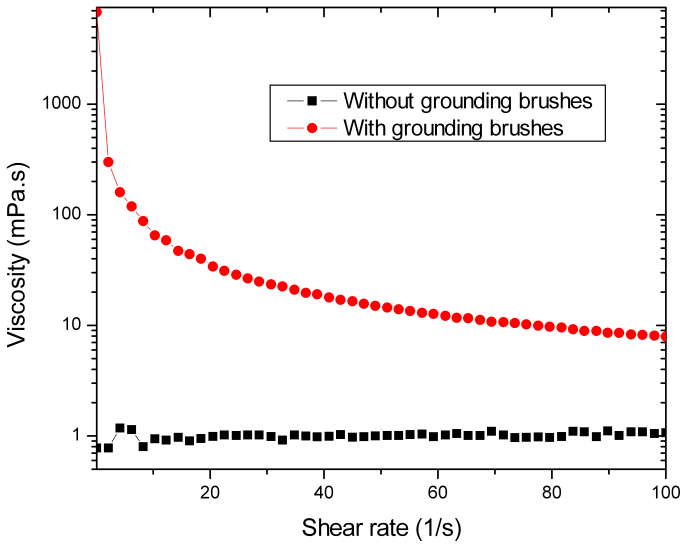

Figure 5.1: The log of viscosity as a function of shear rate for the cell containing distilled water, with and without the metallic brushes touching the cylinder shaft.

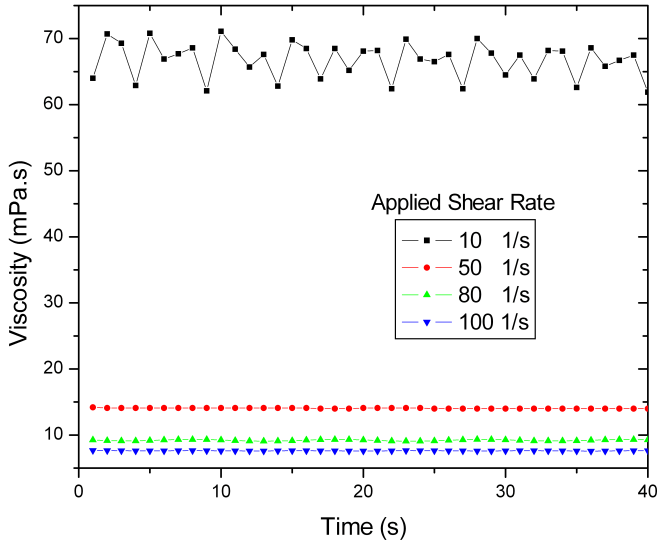

Figure 5.2: The viscosity as a function of time for the cell containing distilled water, sheared at various constant shear rates with the grounding brushes present. The correct viscosity for distilled water is about 1 mPa·s.

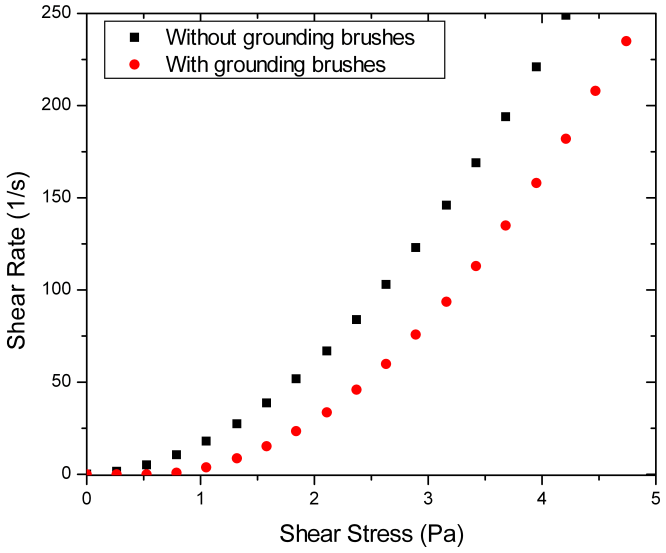

Figure 5.3: The shear rate vs. the applied shear stress with and without the grounding brushes.

The exact effect of the grounding brushes on measurements depends on the configuration of the brushes. If the grounding brushes barely touches the cylinder shaft the contribution will be smaller etc. This must be checked every time before doing measurements with the ERD.

5.2 Rheology of Clay Suspensions

5.2.1 Shear Viscosity

Laponite Suspensions

The flow curves of laponite suspensions with three different volume fractions (Φ =10, 20 and 25 %) are shown in Figure 5.4. The relationship between the shear stress and the shear rate is almost linear. This means that the suspensions behave as Newtonian fluids. According to Equation (3.2), the slope of the curves corresponds to the viscosity of the suspensions.

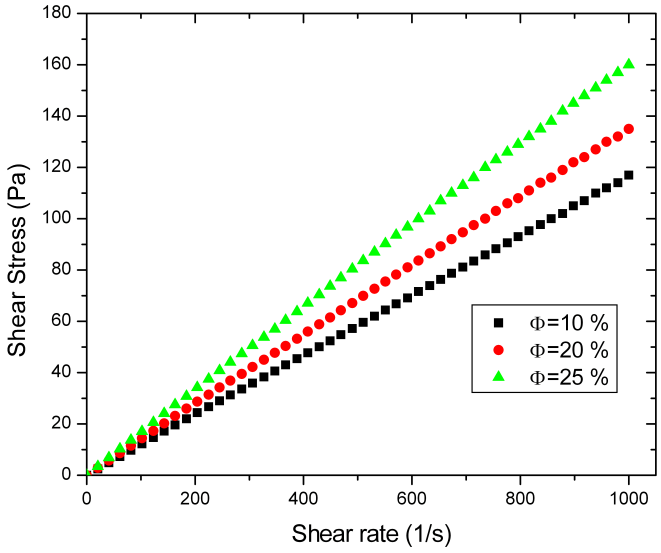

Figure 5.4: The shear stress as a function of shear rate for three different laponite suspensions, Φ =10, 20 and 25 %

NaFH Suspensions

The same Newtonian behavior is also found for the NaFH suspensions, shown in Figure 5.5. Here the flow curves of suspensions with volume fraction Φ^*= 10 and 23 % are shown.

5.2.2 Sedimentation Tests

Laponite Suspensions

Figure 5.6 shows the results of the sedimentation tests for different laponite concentrations. The samples are sheared at a constant shear rate $\dot{\gamma}$=10 $\frac{1}{\mathrm{s}}$ for 2500 seconds, while observing the viscosity. The shape of the curves is quite similar for all concentrations. There is an increase in the viscosities in the beginning, reaching a maximum for $t = 250 - 450$ seconds, then the viscosities gradually decrease. This behavior is especially clear for the highest laponite concentrations. It is clear that the decrease in the viscosity is because particles sediment to the bottom of the cup, making the concentrations of the sheared liquid lower. The sudden increase in the viscosity is more surprising. One explanation of this behavior can be that the shearing causes laponite particles to form large aggregates, which in turn increases the viscosity. Since rheology only gives infor-

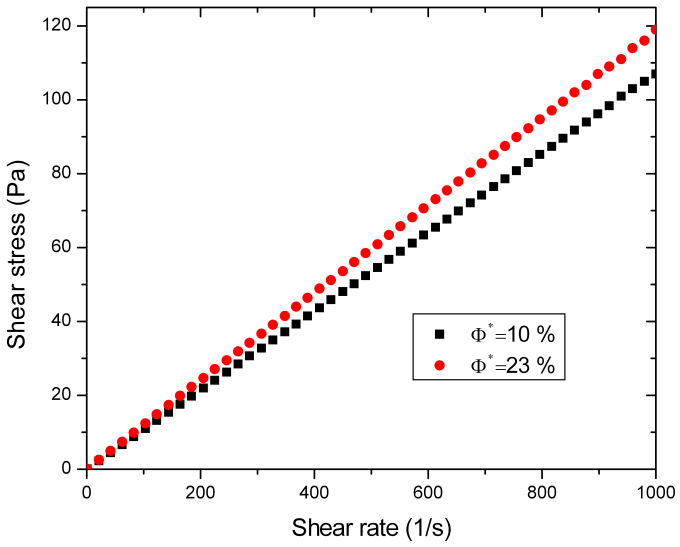

Figure 5.5: Shear stress as a function of shear rate for a Φ^*=10 and 23 % NaFH suspension

mation on the macroscopic behavior of a system, we need to use other techniques to get the exact microscopic behavior.

Another thing we see from Figure 5.6 is that there is a bump in the curves for the three highest concentrations. A reasonable explanation for these bumps can be that the height of the sediment layer at the bottom of the cup is so big that the rotating cylinder comes in contact with it, pushing it away. This can explain why we only see this behavior for the largest concentrations. Several tests were performed in order to investigate the reproducibility of the viscosity curves. They were reproduced quite well.

The most important conclusion from the sedimentation tests is that the concentrations of the samples are clearly changed already after about 15 minutes. This must be considered when performing several measurements in succession. The practical consequence is that the sediment layer must be stirred up between each measurement.

NaFH Suspensions

The sedimentation curves for the three NaFH suspensions, given in Figure 5.7, indicates that these suspensions are more stable than laponite suspensions in terms of sedimentation properties. The highest concentration shows a decrease in the viscosity of only about 3 mPa·s, while the intermediate concentration decrease slightly more. The suspension with the lowest concentration however, has an almost constant viscosity over the

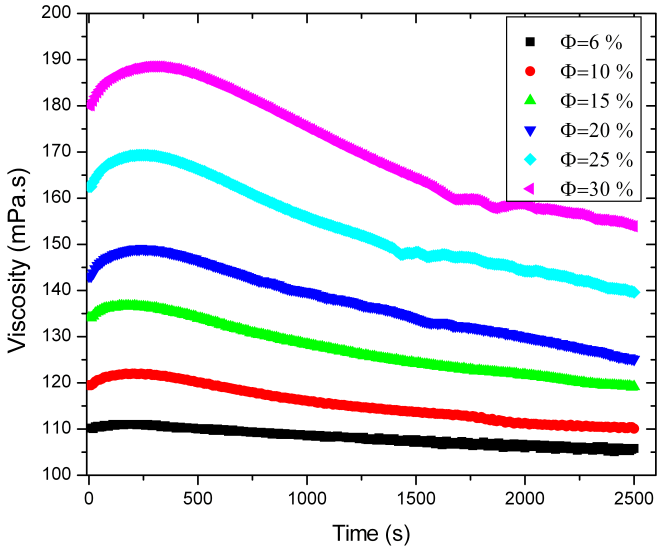

Figure 5.6: The viscosity as a function of time for different laponite particle volume fractions, sheared at $\dot{\gamma}$=10 $\frac{1}{s}$

whole time period. It is reasonable to think that by removing large particle aggregates, sedimentation effects become less dominant. This is exactly what is shown here.

5.3 Rheology of Clay Suspensions in an Electric Field

5.3.1 Static Yield Stress

Laponite Suspensions

Figure 5.8 and 5.9 shows the flow curves, i.e. the shear rate as a function of applied shear stress for the lowest (Φ=6 %) and the highest (Φ=30 %) laponite particle volume fraction, respectively, at different electric field strengths. The electric field has been applied to the sample 5 minutes prior to the shearing in order to form chain- and/or column-like structures across the cylinder gap. These structures must be broken down to make the suspension flow. By applying an increasing shear stress to the sample, the strength in which the structures yield can be identified. This will result in a sudden increase in the shear rate. The corresponding shear stress is taken to be the static yield stress of the sample.

The difference in static yield stresses between the Φ=6 % and Φ=30 % suspension are

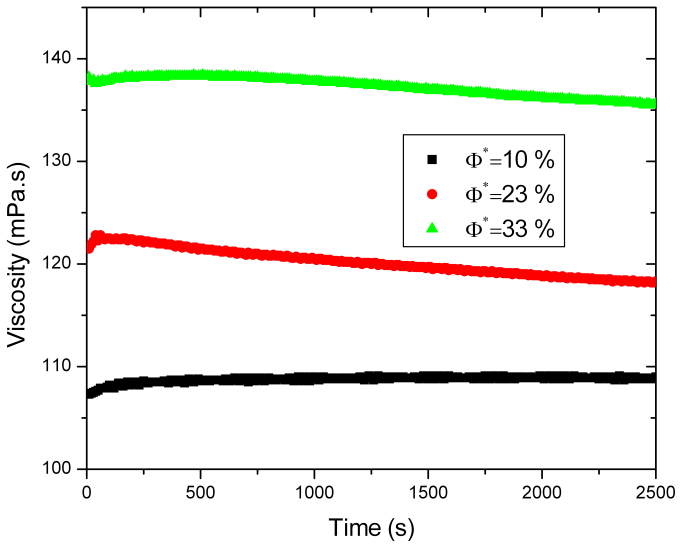

Figure 5.7: Sedimentation tests for NaFH suspensions. The viscosity is plotted as a function of time, shearing the suspensions at a constant shear rate $\dot{\gamma}$=10 $\frac{1}{\mathrm{s}}$.

evident. At the highest electric field strength the static yield stress of the lowest concentration is about 40 Pa, compared to about 190 Pa for highest laponite concentration. The increase in the static yield stress for increasing electric field strength is also clear, e.g. from about 25 Pa at 530 $\frac{\mathrm{V}}{\mathrm{mm}}$ to about 190 Pa at 1770 $\frac{\mathrm{V}}{\mathrm{mm}}$ for the Φ=30 % laponite suspension. The ER effect is generally very small for the two lowest electric fields tested here. This is not surprising since the electric fields are lower than what is considered to be the critical electric field strength E_c ~500-600 $\frac{\mathrm{V}}{\mathrm{mm}}$ for smectites.

Table 5.1 shows the static yield stress values at different electric fields for all the laponite suspensions investigated. In Figure 5.10 the static yield stress is plotted as a function of the electric field strength on a double logarithmic basis. The data is also fitted to the power law $\sigma \propto E^{\alpha}$, shown by the solid lines. The α-values obtained are presented in Table 5.2. The values vary from about 1.65 to 2, with an average of about 1.78.

In order to compare the results of the static yield stress with the results of the yield stress measurements in Section 5.3.2, the static yield stress is plotted as a function of the electric field (log-log) for field strengths higher than 530$\frac{\mathrm{V}}{\mathrm{mm}}$ and fitted to a power law. The exponents obtained are given i Table 5.3. These values range from 1.60 to 1.76, giving an average value of 1.67. This is somewhat lower than when what is obtained when fitting over the whole electric field range, shown in Figure 5.10 and Table 5.2.

Finally the static yield stress normalized by $E^{1.67}$ is plotted as a function of the particle volume fraction on a double logarithmic basis, shown in Figure 5.12. The solid line shows

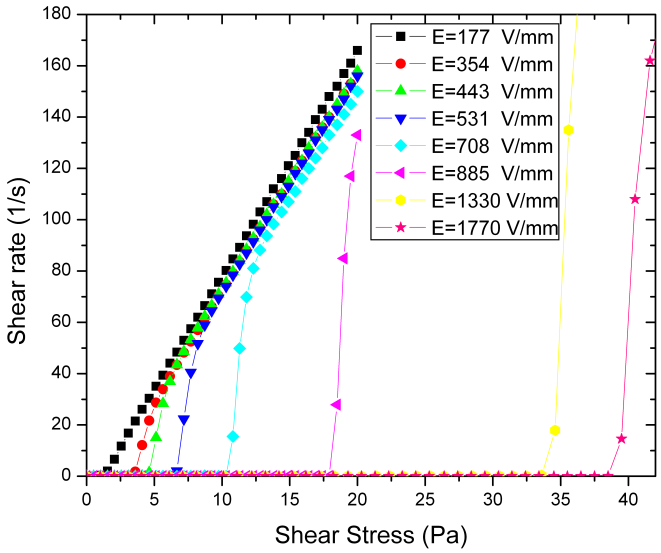

Figure 5.8: The measured shear rate as a function of applied shear stress for a Φ=10 % laponite suspension subject to various electric fields. Static yield stresses are taken where the shear rate jumps from zero to a finite value.

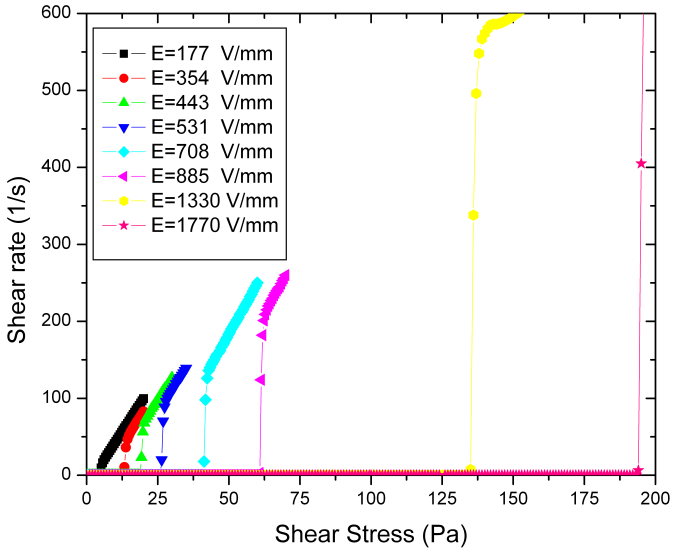

Figure 5.9: The measured shear rate as a function of applied shear stress for a Φ=30 % laponite suspension subject to various electric fields.

Table 5.1: Static yield stress for different laponite concentrations and electric field strengths

E ($\frac{V}{mm}$)	Φ=6 % (Pa)	Φ=10 % (Pa)	Φ=15 % (Pa)	Φ=20 % (Pa)	Φ=25 % (Pa)	Φ=30 %
177	0.5	1.0	2.0	2.0	3.0	3.5
354	2.0	4.5	6.5	8.5	10.5	12.5
442	3.5	6.5	9.0	11.5	17.0	18.0
531	5.5	10.0	12.5	17.5	20.5	25.5
708	9.5	12.5	19.0	25.5	36.0	40.0
885	17.5	21.0	29.5	37.5	53.0	60.0
1330	33.0	39.0	63.0	93.0	102.0	134.0
1720	38.0	64.0	82.0	132.0	152.0	193.0

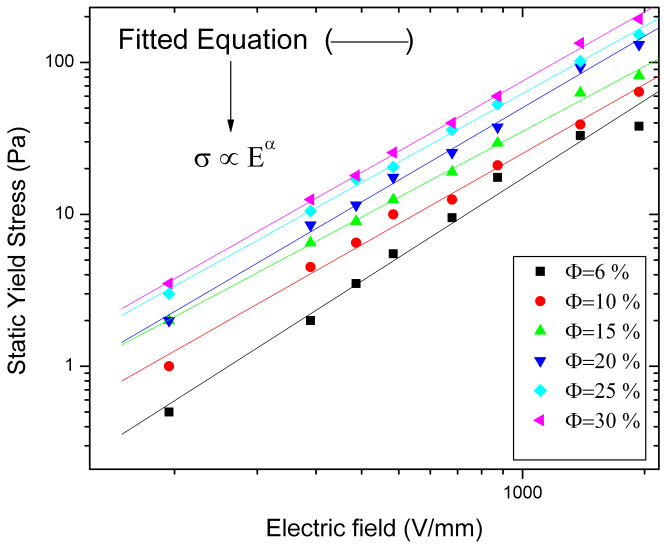

Figure 5.10: Log-log plot of the static yield stress as a function of electric field for various laponite volume fractions. Solids lines shows the fit to the power law $\sigma \propto E^{\alpha}$ for each laponite concentration.

Table 5.2: α-values obtained by the fitting procedure in Figure 5.10

Particle volume fraction Φ (%)	Fitted exponent α
6	1.98±0.10
10	1.76±0.06
15	1.65±0.09
20	1.81±0.05
25	1.71±0.03
30	1.76±0.02

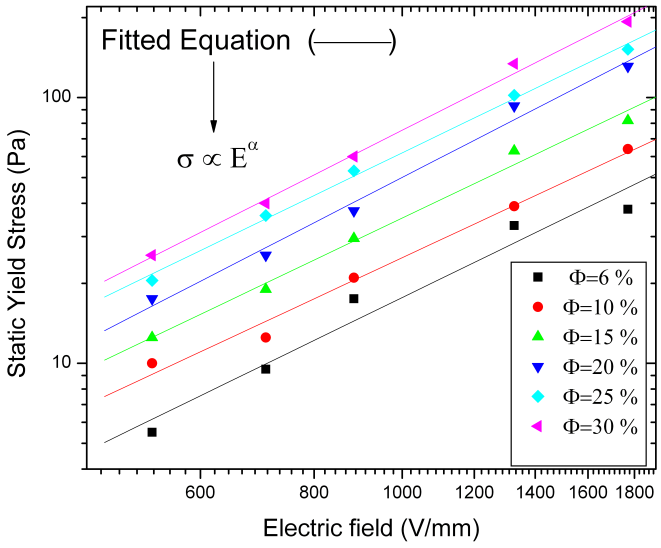

Figure 5.11: Log-log plot of the static yield stress as a function of electric field for various laponite volume fractions in electric fields from 530 to 1770 $\frac{\mathrm{V}}{\mathrm{mm}}$. Solids lines shows the fit to the power law $\sigma \propto E^{\alpha}$ for each laponite concentration.

Table 5.3: α-values obtained by the fitting procedure in Figure 5.11

Particle volume fraction Φ (%)	Fitted exponent α
6	1.67±0.20
10	1.60±0.10
15	1.63±0.09
20	1.76±0.10
25	1.66±0.05
30	1.73±0.06

the power law $\sigma \propto \Phi^{1.10}$.

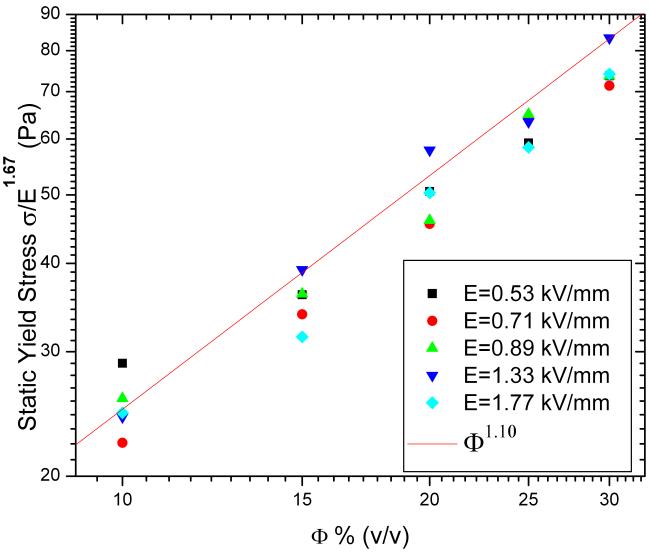

Figure 5.12: Log-log plot of the static yield stress normalized by $E^{1.67}$ as a function of Φ. The data is fitted by the power law $\sigma \propto \Phi^{1.10}$.

5.3.2 Bifurcation Shear Stress

Laponite Suspensions

Figure 5.13 and 5.14 shows the viscosity as a function of time (log-log), sheared at different constant shear stresses for a laponite suspension of particle volume fraction

Φ=10 % at E= 530 $\frac{\text{V}}{\text{mm}}$ and Φ=30 % at E=1330 $\frac{\text{V}}{\text{mm}}$, respectively. The curves have similar shape as the curves produced by the simple physical model of yield stress fluids presented in Figure 3.4.

In Figure 5.13 we see that the viscosity quickly (within 20 seconds) goes to infinity for the lowest applied shear stress (10 Pa). While increasing the applied shear stress the gradual build up in the viscosity to infinity takes longer and longer time. At an applied stress corresponding to 12 Pa the viscosity does not diverge before about 200 seconds. At 13 Pa the viscosity curve has completely changed its shape: instead of increasing toward infinity it is almost constant or slightly decreasing during the time of shearing. Following Bonn et al. [17], the bifurcation shear stress is taken to be the yield stress of the sample. For applied shear stresses higher than the bifurcation shear stress, the viscosity is almost constant at a low value or decreasing during the time of shearing.

The same rheological behavior is also found in Figure 5.14. For stresses lower than the bifurcation shear stress the viscosity diverges discontinuously. For higher stresses we see a thixotropic behavior in a short time period, but after some time the viscosity increases gradually. Perhaps the samples should have sheared for a longer time at the highest electric fields to insure that the viscosity does not diverge. The applied shear stresses are about ten times higher compared to the situation in Figure 5.13 because of much higher laponite particle concentration and electric field strength.

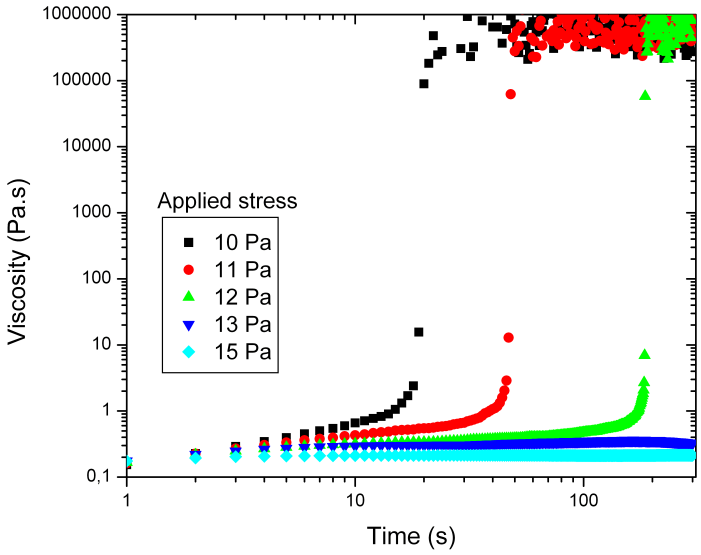

Figure 5.13: Bifurcation in the rheological behavior: viscosity as a function of time for laponite dispersed in silicone oil, particle volume fraction Φ=10 % in an electric field of E=0.53 $\frac{\text{kV}}{\text{mm}}$

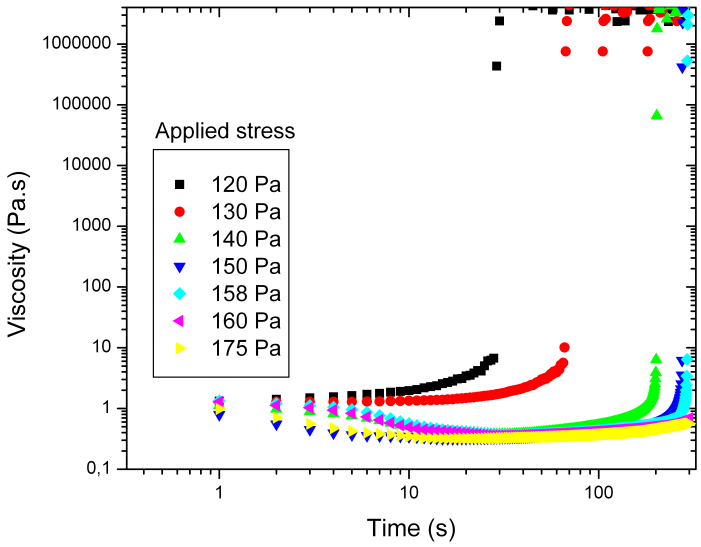

Figure 5.14: Bifurcation in the rheological behavior: viscosity as a function of time for laponite dispersed in silicone oil, particle volume fraction Φ=30 %, in an electric field of E=1.33 $\frac{\text{kV}}{\text{mm}}$

The results of the measured yield stresses for various laponite particle volume fractions and electric field strengths are presented in Table 5.4. The measured yield stresses were reproduced quite well, but they were sensitive to changes in the particle concentration. Some uncertainty in the concentrations between each measurement on the same sample must be expected, in the way the experiments are executed. Based on tests, the uncertainty in the yield stress measurements is estimated to be 2 Pa for electric field strengths less than 1 $\frac{\text{kV}}{\text{mm}}$ and 5 Pa for higher electric fields.

Table 5.4: Yield stress for different laponite concentrations and electric field strengths

E ($\frac{\text{V}}{\text{mm}}$)	Φ=10 % (Pa)	Φ=15 % (Pa)	Φ=20 % (Pa)	Φ=25 % (Pa)	Φ=30 % (Pa)
531	13	18	19	22	30
708	25	28	30	37	50
885	32	38	44	52	77
1330	46	69	90	105	160
1720	64	118	150	160	275

The yield stresses were then plotted as function of electric field strength on a double logarithmic basis and fitted to the power law $\sigma \propto E^{\alpha}$ according to Equation (3.20).

This is shown in Figure 5.15. The solid lines represent the fit to the power law for each laponite concentration. The uncertainty in the measured yield stresses are comparable with the size of measuring points used in the figure. The fits are quite good except for the lowest laponite concentration Φ=10 %. The α-values obtained by the fitting procedure are given in Table 5.5. The α-value for the lowest concentration stands out from the rest, being much smaller, 1.19 compared to 1.54-1.84. One explanation for this can be that the sedimented particles had not been sufficiently dispersed when measuring yield stresses at the highest electric fields. For that reason this concentration will not be subject to any further analysis. The average value for the four highest concentrations is 1.71.

Table 5.5: α-values obtained by the fitting procedure in Figure 5.10

Particle volume fraction Φ (%)	Fitted exponent α
10	1.19±0.12
15	1.54±0.04
20	1.72±0.02
25	1.75±0.03
30	1.84±0.01

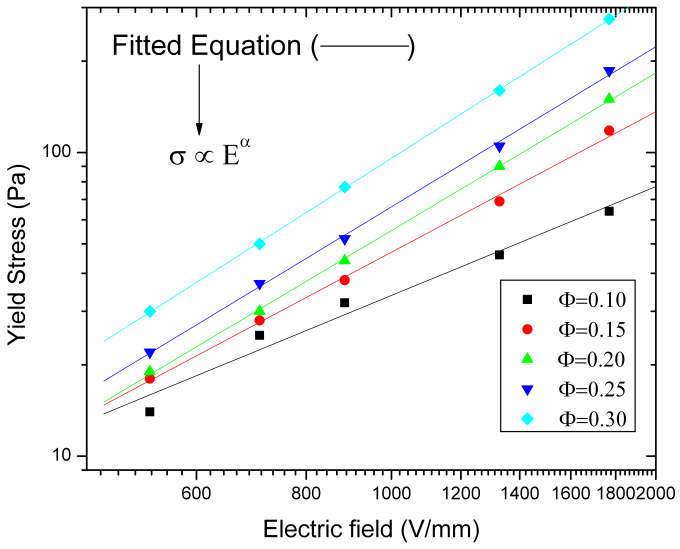

Figure 5.15: Yield stresses as a function of electric field (log-log) for different laponite concentrations. Solid lines are the fit to the power law $\sigma \propto E^{\alpha}$

In Figure 5.16 the yield stress normalized by $E^{1.71}$ is plotted as a function of the particle

volume fraction. For the highest and the lowest concentration there are some spread in the data for different electric fields, while for the middle concentrations the data points coincides well with each other. The data is fitted to the power law $\sigma \propto \Phi^{1.17}$ shown by the solid line.

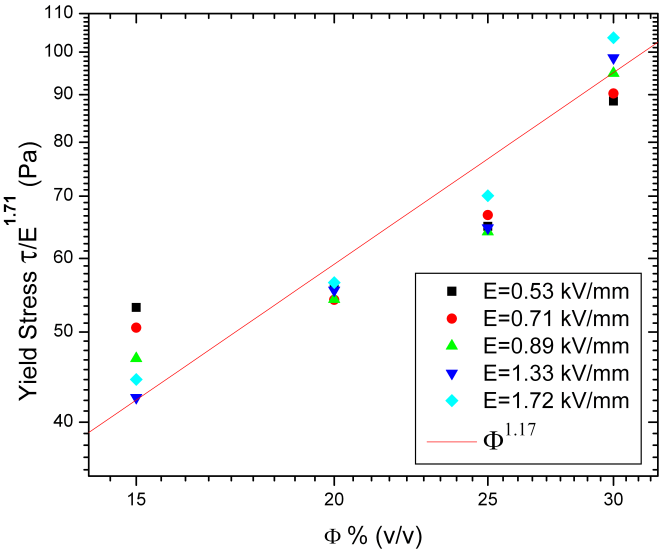

Figure 5.16: Normalized yield stress as a function of particle volume fraction (log-log) together with different power laws

NaFH Suspensions

Figure 5.17 and 5.18 shows the results of yield stress measurements on the NaFH suspension with the highest concentration, at 530 and 885 $\frac{\mathrm{V}}{\mathrm{mm}}$, respectively. Unfortunately yield stresses of NaFH suspensions at higher electric field strengths than E=885 $\frac{\mathrm{V}}{\mathrm{mm}}$ could not be measured , except for the most dilute suspension. The reason was that large currents were running through the system so that the current limitation in the voltage supply was reached, thus reducing the electric field.

The measured bifurcation shear stresses are shown in Table 5.6. Since the volume fractions of the suspensions are lower then indicated and unknown, the yield stresses can not be directly compared with corresponding laponite suspensions. However, it is possible to say something general about the ER effect of the NaFH suspensions. The measurements indicate that the ER effect is weaker than for laponite suspensions. The yield stresses also seems as if they have a weaker dependence on the electric field strength, at least for the relative moderate electric field strengths used here. In Figure 5.19 the yield stresses

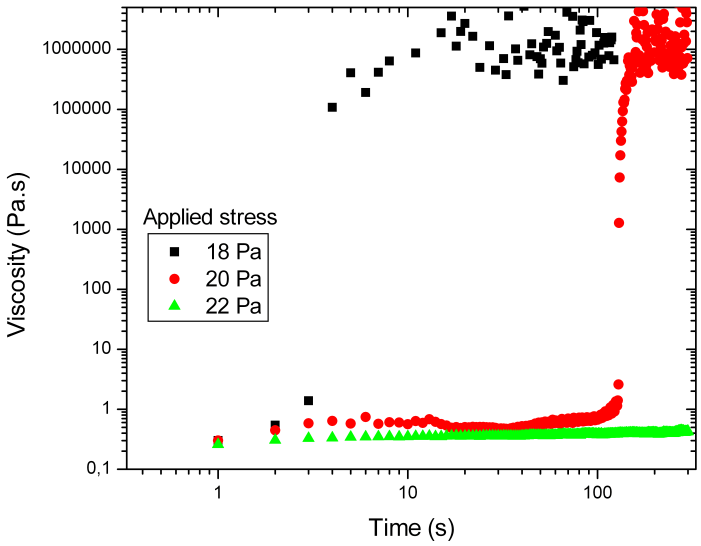

Figure 5.17: Viscosity as a function of time for the NaFH suspension with the highest particle volume fraction at E=530 $\frac{\mathrm{V}}{\mathrm{mm}}$, for different applied shear stresses.

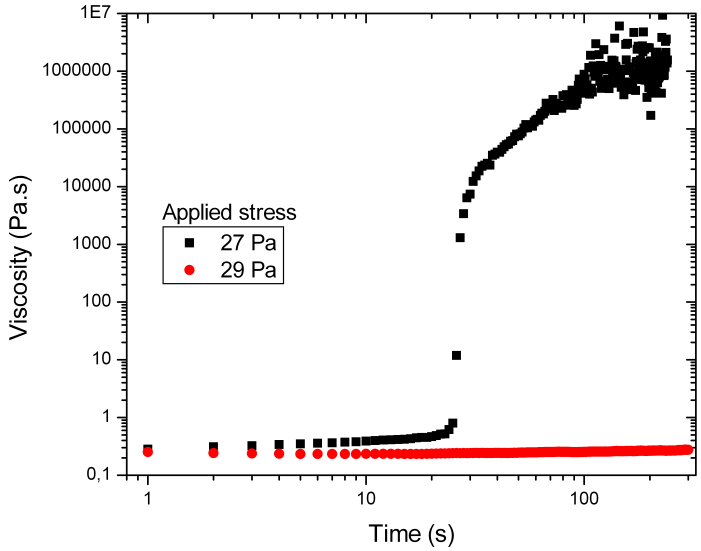

Figure 5.18: Viscosity as a function of time for the NaFH suspension with the highest particle volume fraction at E=885 $\frac{\mathrm{V}}{\mathrm{mm}}$, for different applied shear stresses.

are plotted as a function of the electric field on log-log scale. The data is again fitted to the power law E^{α} shown by the solid lines. The α-values obtained are 1.53 for the lowest concentration, 1.07 for the intermediate concentration and 0.54 for the highest. The error in the two highest concentrations is very big, since only three measuring points have been used in the fitting. Since the concentrations are unknown, the yield stresses have not been plotted as a function of the particle volume fraction.

K. Palmar found an electric field dependence of 1.58 when measuring static yield stresses on similar suspensions [57]. The volume fraction dependence of the yield stress was also analyzed, and found to be 0.54.

Table 5.6: The bifurcation shear stress for different NaFH concentrations and electric fields strengths. Φ^* indicates that the real volume fractions are lower.

E ($\frac{V}{mm}$)	Φ^*=10 % (Pa)	Φ^*=23 % (Pa)	Φ^*=33 % (Pa)
531	3	8	21
708	4	10	23
885	6	14	28
1330	12	–	–
1720	17	–	–

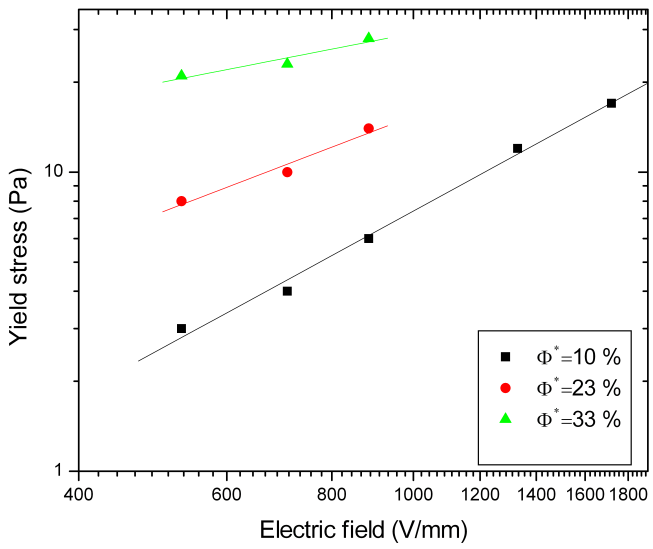

Figure 5.19: Bifurcation yield stress as a function of the electric field for three different NaFH suspensions. The data is fitted to a power law shown by the solid lines.

Chapter 6

Conclusion

6.1 Electrorheology of Laponite Suspensions

The static yield stresses measured in Section 5.3.1 are in general smaller than the bifurcation shear stresses presented in Section 5.3.2 when comparing equal concentrations and electric field strengths. The only exceptions are the two highest electric fields for the lowest concentration, where the static yield stresses are higher.

This may be surprising because when measuring the static yield stress the suspension has been at rest and chain- and/or column-like structures can form uninterrupted without any shearing for 5 minutes. So when the shearing starts, the structures ought to be strong and compact. On the other hand, when measuring the bifurcation shear stress the polarized laponite particles/aggregates must compete with the shearing force in order to form chains across the gap. The bifurcation shear stress will correspond to the situation when the interaction forces between particles and the shearing force are equal. For lower stresses the gradual formation of chains will at last prevent shearing of the suspension and the viscosity goes to infinity.

The two measurements are in fact very different. When measuring the static yield stress, one measure what applied shear stress is needed to break up structures already present in the fluid. The bifurcation shear stress on the other hand, is the minimum stress where solid structures can form during shearing.

When it comes to the electric field dependence of the yield stress, E^{α}, the two methods gives quite equal results when comparing the average values: 1.67 for the static yield stress and 1.71 for the bifurcation shear stress method. However, for the latter method the spread in the data is bigger and the lowest concentration has been disregarded. The two methods also gives quite equal particle volume fraction dependence, Φ^{β}, of the yield stress with an exponent $\sim$1.1.

These results differ slightly from what PhD. K. Palmar found when measuring the static

yield stress of laponite suspensions (Φ =18-49 %) in electric fields from 1.33 to 3.54 $\frac{\text{kV}}{\text{mm}}$ [53]. He found α-values between 1.72 and 1.94, with an average of value of 1.85 and β=1.70. However, the results are not necessarily comparable since he measured in intermediate/high electric field range and I measured in a low/intermediate range, and the ER behavior is expected to be different in these ranges.

The measured electric field dependence of the electric field, the exponent α, agrees with what is found in the nonlinear conduction theory for spherical particles. This theory predicts α=2 for low electric fields and α=1.5 for the high electric fields. The transition is expected to be abrupt. So when fitting the yield stress over the whole electric field range we should expect an exponent close to 1.75, the average of the two values. This is indeed the result of the measurements presented here, where the exponents have been fitted in the low/intermediate electric field region. The measured static stresses show a near linear relationship with the particle volume fraction. This is in agreement with what is predicted by the simple polarization theory.

The polarization of clay particles by the DC electric field may be caused by migration of surface charges, but also the movement of interlayer cations Na^+ may contribute to the polarization.

6.2 Electrorheology of NaFH Suspensions

For the NaFH suspensions, bifurcation yield stresses were only measured in a low electric field region, except for the most dilute suspension, due to instrumental limitations in the voltage supply when large currents were running in the samples. The electric field dependence of the yield stress was found to be $\sim$1.5 for the sample with lowest NaFH concentration. The other samples show a weaker dependence, but no certain conclusions can be made because of few measuring points. The obtained value is close to what K.Palmar found when measuring the static yield stress of the same suspension [57].

Generally the ER effect seems to be lower for the NaFH suspensions than for laponite suspensions.

The volume fraction dependence of the bifurcation yield stress has not been investigated here, due to limited number of measuring points and the fact that the exact volume fractions of the suspensions are unknown.

Bibliography

[1] B. Schjelderupsen. Preparation for: A Rheological Study of Nano-Layered Silicates in an External Electric Field. Project work NTNU, 2006.

[2] F. Bergaya, B.K.G. Theng, and G. Lagaly. *Handbook Of Clay Science*. Elsevier, 2006.

[3] J.O. Fossum. Physical Phenomena in Clays. Talk given at The National Norwegian Broadcasting (P2) `http://folk.ntnu.no/fossumj/P2Akademiet/english.htm`, Feb 2000.

[4] G.J. da Silva, J.O. Fossum, E. DiMasi, K.J Måløy, and S.B. Lutnæs. Synchrotron x-ray scattering studies of water intercalation in a layered synthetic silicate. *Phys. Rev. E*, **66**:011303, 2002.

[5] E. DiMasi, J.O. Fossum, T. Gog, and C. Venkataraman. Orientational order in gravity dispersed clay colloids: A synchrotron x-ray scattering study of Na fluorohectorite suspensions. *Phys. Rev. E*, **64**:061704, 2001.

[6] W.M. Winslow. Induced Fibration of Suspensions. *J. Appl. Phys.*, (20):1137–1140, 1949.

[7] T. Hao. Electrorheological Fluids (review). *Adv. Mater.*, **13**(24):1848–1857, 2001.

[8] W. Wen, X. Huang, S. Yang, K. Lu, and P. Sheng. The giant electrorheological effect in suspensions of nanoparticles. *Nature*, **2**:727–730, 2003.

[9] W. Wen, X. Huang, and P. Sheng. Particle size scaling of the giant electrorheological effect. *Appl. Phys. Lett,*, **85**:299–301, 2004.

[10] H.A. Barnes, J.F. Hutton, and K. Walters. *An Introduction to Rheology*. Elsevier, 1989.

[11] R.G. Larson. *The Structure and Rheology of Complex Fluids*. Oxford, 1999.

[12] G. Strobl. *Condensed Matter Physics*. Springer, 2004.

[13] G. Schramm. *A Practical Approach to Rheology and Rheometry*. Haake Instruments Inc., 2000.

[14] E.C. Bingham. *Fluidity and Plasticity*. McGraw-Hill, 1922.

[15] P. Møller, J. Mewis, and D. Bonn. Yield stress and thixotropy: on the difficulty of measuring yield stress in practice. *Soft Matter*, **2**:274–283, 2006.

[16] A.E. James, D.J.A. Williams, and P.R. Williams. Direct measurement of static yield properties of cohesive suspensions. *Rheology Acta*, **26**:437–446, 1987.

[17] P. Coussot, Q. D. Nguyen, H. T. Huynh, and D. Bonn. Avalanche Behavior in Yield Stress Fluids. *Physical Review Letters*, **88**(17):175501–+, 2002.

[18] F.K. Liu and C.C. Mei. Slow spreading of a sheet of Bingham fluid on an inclined plane. *Journal of Fluid Mechanics*, **207**:505–529, 1989.

[19] H. See. Advances in Modelling the Mechanisms and Rheology of Electrorheological Fluids. review. *Kor-Aust. Rheo. J.*, **11**(3):169–195, 1999.

[20] J.E. Stangroom. Electrorheological Fluids. *Phys. Technol.*, **14**:290–296, 1983.

[21] H. See, H. Tamura, and M. Doi. The Role of Water Capillary Forces in Electro-Rheological Fluids. *J.Phys D: Appl. Phys*, **26**:746–752, 1993.

[22] H. Tamura, H. See, and M. Doi. Model of porous particles containing water in electro-rheological fluids. *J.Phys D: Appl. Phys*, **26**:1181–1187, 1993.

[23] D.L. Klass and T.W. Martinek. Electroviscous Fluids I: Rheological Properties. *J. Appl. Phys.*, **38**:1181–1187, 1967.

[24] D.L. Klass and T.W. Martinek. Electroviscous Fluids II: Electrical Properties. *J. Appl. Phys.*, **21**:1181–1187, 1967.

[25] H. Block and J.P. Kelly. Electro-rheology. *J.Phys D: Appl. Phys.*, **21**:1661–1677, 1988.

[26] J. Hemp. Theory of dilute electro-rheological fluidsy. *Proc.R.Soc.Lond.A*, **21**:297–315, 1998.

[27] M. Parthasarathy and D.J. Klingenberg. Electrorheology: Mechanisms and Models. review. *Mat. Sci. Eng.*, **R17**:57–103, 1996.

[28] D.J. Griffiths. *Introduction to Electrodynamics*. Prentice Hall, 1999.

[29] R.A. Anderson. Effect on Finite Conductivity in Electrorheological Fluids. In R. Tao, editor, *Int. Conf. on Electrorheological fluids: mechanisms, properties, structure and applications*, pages 81–90, Carbondale, Illinois, USA, Oct. 15-16, 1991. 1992. World Scientific.

[30] L.C. Davis. Finite-Element Analysis of Particle-Particle Forces in Electrorheological Fluids. *Appl. Phys. Lett.*, **60**(3):319–312, 1992.

[31] P. Atten, J.N. Foulc, and N. Felici. A conduction model of the electrorheological effect. *Int. J. Phys. B*, **8**:2731–2745, 1994.

[32] T.B. Jones. *Electromechanics of Particles.* Cambridge University Press, 1995.

[33] B. Khusid and A. Acrivos. Effects of conductivity in electric-field-induces aggregation in electrorheological fluids. *Phys. Rev. E*, **52**:1669–1693, 1995.

[34] N. Felici et al. A Conduction Model of Electrorheological Fluids. In R. Tao and G.D. Roy, editors, *Int. Conf. on Electrorheological fluids: mechanisms, properties, structure and applications*, pages 139–152, Feldkirch, Austria, July 20-23, 1993. 1994. World Scientific.

[35] J.N. Foule and N. Felici. Microscopic Model of Interactions between Particles in an Electrorheological Fluid. *J. Elec.Stat.*, **33**:103–112, 1994.

[36] L.C. Davis. Time-dependent and nonlinear effects in electrorheological fluids. *Appl. Phys. Lett.*, **81**:1985–1991, 1997.

[37] L.C. Hyoung, S.C. Min, and W.J Kim. Electrorheology and universal yield stress function of semiconducting polymer suspensions. *Kor.-Aust Rheo. J.*, **13**:197–203, 2001.

[38] H. Block and J.P. Kelly. Materials and Mechanisms in Electrorheology. *Langmuir*, **6**:6–14, 1990.

[39] D.J. Klingenberg and C.F. Zukoski IV. Studies on the Steady-Shear Behavior of Electrorheological Suspensions. *Langmuir*, **6**:15–24, 1990.

[40] Y.H Shih and H. Conrad. Influnce of Particle Size on the Dynamic Strength of Electrorheological fluids. *Int. J. Mod. Phys. B*, **8**:2835–2853, 1994.

[41] C.W Wu and H. Conrad. Influence of mixed particle size on electrorheological response. *J. Appl. Phys.*, **83**:3880–3884, 1998.

[42] K. Asano, H. Suto, and K. Yatsuzuka. Influence of the particle configuration on electrorheological effect. *J. Elec.Stat.*, **40-41**:573–578, 1997.

[43] R.C. Kanu and M.T. Shaw. Enhanced Electrorheological Fluids Using Anisotropic Particles. *J. Rheol.*, **42**:657–670, 1998.

[44] X. Duan, L. Weili, H. Chen, and Y He. The Effect of Particle Shape on Water-Free Mica ER Fluids. *J. Int. Mat. Struc.*, **11**:43–46, 2000.

[45] Building the phyllosilicates.
`http://pubpages.unh.edu/~harter/crystal.htm` (5 May 2007).

[46] B. Velde. *Origin and Mineralogy of Clays.* Springer, 1995.

[47] Phyllosilicates.
`http://www.geoclassroom.com/mineralogy/phyllosilicates.html`
(9 May 2007).

[48] J.O. Fossum. Physical phenomena in clays. *Physica A*, **270**:270–277, 1999.

[49] L. Jyotsana. Interaction of Polymer with Clays. *J. Appl. Cryst.*, **33**:673–676, 2000.

[50] Laponite.com. Brochure.
`http://www.laponite.com/pdfs/laponite.pdf` (9 May 2007).

[51] M.W. Kroon, L. Vos, and G. H. Wegdam. Structure and Formation of a Gel of Colloidal Disks. *Langmuir*, **57**(2):1962–1971, 1998.

[52] S. Bhatia, J. Barker, and A. Mourchid. Scattering of Disklike Particle Suspensions: Evidence for Repulsive Interactions and Large Length Scale Structure from Static Light Scattering and Ultra-Small-Angle Neutron Scattering. *Langmuir*, **19**(3):532–535, 2003.

[53] K.P.S Parmar. *Electrorheological suspensions of laponite in oil: rheometry studies under steady shear.* PhD thesis, NTNU, 2006.

[54] C.W. Wu and H. Conrad. The Temperature Dependence of the Conductivity of Silicone Oil and Related Electrorheology of Suspensions Containing Zeolite Particles. *J. Appl. Phys.*, (31):3403, 1998.

[55] Swedish Chemicals Agency KEMI. Information on substances.
`http://apps.kemi.se/flodessok/floden/kemamne_eng/siloxaner_eng.htm`
(11 May 2007).

[56] Anton Paar. Physica MCR 300 Brochure.
`http://www.houm.no/pdf/mcr_serie_e.pdf` (22 April 2007).

[57] K.P.S Parmar. *Electrorheology of Synthetic Na-Fluorohectorite Clay Particles Suspended in Oil: Rheometry Studies under Steady Shear.* PhD thesis, NTNU, 2006.